EUROPEAN ORGANIZATION FOR NUCLEAR RESEARCH

CERN-EP/80-134
29 July 1980

A LARGE MAGNETIC SPECTROMETER SYSTEM FOR HIGH-ENERGY MUON PHYSICS

The European Muon Collaboration
[CERN[1]-DESY (Hamburg)[2]-Freiburg[3]-Kiel[4]-Lancaster[5]-LAPP (Annecy)[6]-
Liverpool[7]-Oxford[8]-Rutherford[9]-Sheffield[10]-Turin[11]-Wuppertal[12]]

J.J. Aubert[6], G. Bassompierre[6], K.H. Becks[12], Y. Bertsch[6], C. Besson[6], C. Best[1], E. Böhm[4], D.R. Botterill[9], F.W. Brasse[2], C. Broll[6], J. Carr[9], B. Charles[9], R.W. Clifft[9], J.H. Cobb[5], G. Coignet[6], F. Combley[10], J.M. Crespo[6], P.F. Dalpiaz[11], P. Dalpiaz[11], W.D. Dau[4], J.K. Davies[8], Y. Declais[6], R.W. Dobinson[1], J. Drees[12], A. Edwards[7], M. Edwards[9], J. Favier[6], M.I. Ferrero[11], J.H. Field[1,a], W. Flauger[2], E. Gabathuler[1], R. Gamet[7], J. Gayler[2], P. Ghez[6], C. Gössling[2], J. Haas[3], U. Hahn[3,b], K. Hamacher[12], P. Hayman[7], M. Henckes[12], H. Jokisch[4], J. Kadyk[6,c], V. Korbel[2], M. Maire[6], L. Massonnet[6], A. Melissinos[1,d], W. Mohr[3], H.E. Montgomery[1], K. Moser[3], R.P. Mount[8], M. Moynot[6], P.R. Norton[9], A.M. Osborne[1], P. Payre[1], C. Peroni[11], H. Pessard[6], U. Pietrzyk[12], K. Rith[1], M.D. Rousseau[9], E. Schlösser[3], M. Schneegans[6], T. Sloan[5], M. Sproston[9], W. Stockhausen[12], H.E. Stier[3], J.M. Thénard[6], J.C. Thompson[9], L. Urban[6], M. Vivargent[6], G. Von Holtey[1], H. Wahlen[1], E. Watson[1], V.A. White[1], D. Williams[7], W.S.C. Williams[8] and S.J. Wimpenny[10]

Geneva - July 1980

(Submitted to Nuclear Instruments and Methods)

---

a) Now at DESY, Hamburg, Germany.

b) Now at Rheinmetall, Düsseldorf, Germany.

c) On sabbatical leave from LBL, Berkeley, California, USA.

d) On sabbatical leave from Rochester University, Rochester, NY, USA.

ABSTRACT

The European Muon Collaboration has built a large magnetic spectrometer system for deep inelastic muon scattering experiments at the CERN SPS muon beam. The general characteristics of the apparatus -- composed of a target of either liquid hydrogen or deuterium, or iron plus scintillator, followed by a large magnet with wire chambers before and after it for precise angle and momentum measurement, a muon identifier, large trigger hodoscopes, and hadron identifiers -- are explained and each part is described in some detail. The main features of the data-acquisition and apparatus-monitoring systems and of the off-line event reconstruction are given.

CONTENTS

1. INTRODUCTION

Deep inelastic muon scattering provides a clean method of studying the constituents of the nucleon, since the virtual photon can interact directly with the charged partons or quarks. The space-time scale to which the nucleon is probed is determined by the four-momentum transfer (Q^2) of the exchanged photon. The installation of a high-quality muon beam at the CERN Super Proton Synchrotron (SPS) has opened up the possibility of performing high-statistics experiments at energy transfers up to $\nu \approx 250$ GeV and four-momentum transfers up to $Q^2 \approx 200$ $(GeV/c)^2$. The data should provide tests of the predictions of the theory of the strong interactions, the quantum chromodynamics.

The main aims of the experimental programme of the European Muon Collaboration (EMC) are:

- Measurement of the deep inelastic structure function νW_2 for both proton and neutron, and an investigation of the pattern of scaling violation.
- Separation of the longitudinal (σ_L) and transverse (σ_T) virtual photon cross-sections as a function of Q^2 and ν.
- Studies of charged and neutral hadrons produced in the inelastic collisions.
- Study of inclusive production of multimuons in a search for new phenomena in the vector meson and charmed meson production. To achieve high luminosity, a heavy target is used for these measurements.

To pursue the above programme, the EMC has designed[1] and built a versatile spectrometer facility capable of accepting and analysing the scattered muon together with the charged hadrons and photons produced, over a wide range of angles and momenta. The apparatus has been constructed in two separate phases. The first phase, the forward spectrometer, which is described in this report, was built in the various laboratories of the EMC and has been operational for nearly two years (experiment NA2). The second phase, the vertex detector, is at present under construction and will be the subject of a separate report.

2. GENERAL FEATURES OF THE SPECTROMETER SYSTEM

The forward spectrometer (FS) was designed to have a large acceptance for the scattered muon and also to be able to analyse hadrons produced in the forward hemisphere. An important feature is its ability to be triggered on events in a selected part of the Q^2-ν plane, using only the scattered muon. Figure 1 shows a Q^2-ν plot for E = 280 GeV incident muon energy; some lines of constant θ (muon scattering angle), $x = Q^2/2M\nu$ (the Bjorken scaling variable), $W = \sqrt{s}$ (the photon-nucleon centre-of-mass energy) are shown; the values of E' (the scattered muon energy) are also shown. Since the muon-nucleon cross-section has a very strong Q^2 dependence ($\approx 1/Q^4$), where $Q^2 = 4EE' \sin^2 \theta/2$, it is essential that these variables are accurately measured. The incident beam momentum being measured to $\approx 0.5\%$, a measurement of the scattered muon momentum should approach the same precision.

To achieve the desired resolution in Q^2 and ν, the spectrometer (see figs. 2 and 3) was designed on the lever-arm principle, using a conventional large-window dipole magnet (FSM) and drift chambers in front ($W_{1,2}$) and behind ($W_{3,4,5}$). To maximize the acceptance, the target (liquid H_2/D_2 or iron plus scintillator) is put as close as possible to the FSM, leaving a lever-arm of 0.6 m between the drift chambers W_1 and W_2. Proportional chambers P_1, P_2, P_3, inside the FSM, provide tracking through the magnet. Their resolving time, shorter than that of W_1 and W_2, helps to remove out-of-time tracks mainly due to low-energy electrons produced in the target. A distance of 5 m between chambers W_3 and $W_{4,5}$ together with chambers W_1 and W_2 gives a momentum resolution of the order of $\pm 10^{-4}$ p GeV/c with 5 T·m bending power and ± 0.3 mm spatial resolution in the drift chambers. The 5 m space between the rear chambers allows the insertion of a multi-cell Čerenkov counter $\check{C}_2$ to give identification of pions, kaons, and protons in some momentum ranges.

The scattered muon is identified by the presence after 2.5 m of iron of a track, reconstructed in four layers of large drift-chamber modules $W_6(1,2)$ and $W_7(1,2)$, which links up with a track in $W_{4,5}$. The first five interaction lengths

of the absorber consist of the lead and iron of the calorimeter H_2, and the following ten interaction lengths of magnetized iron which absorbs most of the hadrons which do not decay upstream.

The angular acceptance of the spectrometer is $\pm 8^\circ$ in the bending plane for scattered muons of $E' > 15$ GeV and $\pm 5^\circ$ in the vertical plane, allowing most hadrons of positive x_F ($x_F = p_L^*/\sqrt{s}$) to be accepted. In order to operate with muon rates up to 5×10^7 particles/s, all detectors were made insensitive in the beam region except for specially constructed fast counters and chambers on the beam line.

Scintillator hodoscopes in the last vertical bend of the beam line (BMS), measure the momentum of each beam muon to $\sim \pm 0.5\%$. The beam dimensions being rather large , two fast beam hodoscopes, one after the last bending magnet of the beam (BH_a) and the other (BH_b) just in front of the target, give the position and angle of the incoming muon with a precision of ± 1.0 mm and ± 0.2 mrad. Another hodoscope (H_5), downstream of the apparatus, is used to monitor the beam intensity. Two proportional chambers P_{0a} and P_{0b}, placed between the target and the magnet, allow the reconstruction of the trajectories of the muons scattered at small angles which are in the insensitive areas of the large chambers.

Several simultaneous conditions are imposed on the scattered muon in order to obtain an electronic trigger with a good rejection of background events. The main sources of background are halo muons, knock-on electrons and hadron punch-through in the absorber. These trigger conditions are imposed by selecting specific combinations of the elements of the large hodoscopes H_1, H_3, and H_4 together with the veto counters V_1, V_2, and V_3.

To avoid high single rates due to knock-on electrons from the target no trigger counter is placed in front of the FSM. To reduce the contribution of the beam halo to the trigger, suitable elements of H_1 and H_3 are chosen to require pointing of the scattered muon to the target region. The system of veto counters helps to bring the triggers by halo muons to a negligible level. The rate of false triggers initiated by muons from π decays can be reduced by requiring a minimum scattered muon momentum. This is achieved by requesting suitable

combinations of the elements of H_3H and H_4H which are after the magnetized absorber. This momentum cut ($\approx$ 15 GeV/c) sets an upper limit to the range of ν which can be explored.

Once the above backgrounds have been suppressed, the final trigger rate is reduced to an acceptable level by imposing a minimum scattering angle requirement on the muon, using elements of H_1 and H_3. It can be seen from fig. 1 that low Q^2 events can be excluded with little momentum dependence if the angle cut is smaller than $\sim 2^\circ$.

The high muon flux and the aim to accumulate large numbers of unbiased events causes the trigger rates to be rather high. Therefore, a powerful data acquisition and apparatus monitoring system, based on four DEC PDP 11/70 computers, was designed.

3. DESCRIPTION OF THE APPARATUS

3.1 Muon beam line

The experiment is situated on the SPS muon beam line M2 [2]. Muons are produced by decay in flight of charged pions and kaons emitted from the bombardment of a primary target with 400 GeV/c protons. This beam is designed to operate in the momentum range 50-300 GeV/c. The main features of the beam line (fig. 4) are:

a) A front end, which accepts parent pions and kaons within an energy-dependent solid angle of 10-20 μsr centred on zero degrees production angle from the primary target, and then separates off the unused primary protons. A momentum band $\Delta p/p(\pi,K) \lesssim \pm 10\%$, which matches the input of the following FODO channel, is selected.

b) A decay channel, 600 m long, composed of a regular array of large-aperture quadrupoles alternatively focusing and defocusing. This FODO array is designed to contain with minimum losses both parent pions and kaons of mean momentum $p(\pi,K)$ and also all decay muons, i.e. $0.57 \times p(\pi) < p(\mu) < p(\pi)$.

c) A hadron absorber which removes most of the pions and kaons remaining at the end of the decay channel. To minimize multiple scattering of the muons, the absorber is made of beryllium, 10 m long, and to minimize beam emittance it is located at a focus within the apertures of the momentum selecting magnets. The

predicted π/μ ratio just after the absorber is $\sim 10^{-6}$, compared with an upper limit of 10^{-5} measured at the experiment for $p(\mu) = 280$ GeV/c.

d) A back end which selects muons and transports them to the experiment. It consists of a vertical bend (24 mrad), which together with the following elements selects an effective momentum band of $\Delta p/p(\mu) \approx \pm 5\%$, a 250 m FODO array, and a compensating bend which removes dispersion and provides the basis of a spectrometer to measure the beam momentum (see section 3.4.1). Finally, a series of magnets is used to produce the required beam conditions at the target.

The fluxes measured at the experiment, per proton of 400 GeV incident on the 50 cm beryllium primary target, are $\approx 3.8 \times 10^{-5}$, $\approx 1.4 \times 10^{-5}$ and $\approx 1.8 \times 10^{-6}$ positive muons for mean muon momenta of 120, 200, and 280 GeV/c, respectively. For negative muons, the fluxes are lower by a factor of 2.5 to 5, for momenta ranging from 120 to 280 GeV/c. Intensities of $\lesssim 3 \times 10^{7}$/s have so far been used in the experiment, although a much higher rate can be handled by the beam line. The emittances measured at the front of the experiment vary slightly with momentum between 120 and 280 GeV/c; the r.m.s. dimensions vary from 15 to 20 mm and the r.m.s. divergences from 0.4 to 0.5 mrad vertically and 0.2 to 0.4 mrad horizontally. An r.m.s. width of the momentum distribution, as measured by the beam momentum station (BMS), is $\sim (4.5 \pm 0.5)\%$.

In order to reduce the beam halo, a system of magnetic collimators, installed downstream of the absorber bend, deflects away unwanted muons. The collimators are each independently adjusted to cut a little into the beam, enabling the beam-to-halo ratio to be optimized. The halo particles remaining within the acceptance of the apparatus are recorded by the three scintillation counter arrays: V_1, V_2, and V_3, upstream of the experiment (see fig. 3). The measured rate of halo muons traversing V_3 and the back hodoscope H_4, is $\sim 7\%$ of the beam rate at 280 GeV/c. In addition there is a soft component associated with the beam which produces a singles rate in V_3 of $\sim 20\%$ of the beam intensity.

3.2 Targets

Two types of target, located in the space between BH_b and P_{0a} (see fig. 3), are used: a 6 m vessel filled with liquid hydrogen or deuterium, or a 4.75 m iron-scintillator target (STAC).

3.2.1 Liquid hydrogen/deuterium target

The liquid hydrogen or deuterium target used in the NA2 experiment has a length of 6 m and a 15 cm diameter. The target cell, made of 0.13 mm stainless steel, is insulated by $\sim$ 70 layers of "super-insulation" and supported on five discs of "Rohacell" within its vacuum vessel.

The vacuum vessel is made of an aluminium alloy of a thickness varying from 5 mm at the upstream end to 2.5 mm at the downstream end. A hemispherical end cap of thickness varying from 2.5 mm to 1.0 mm on the target axis is used to enclose the downstream end. This presents the minimum thickness of material possible (consistent with safety requirements) to scattered particles and also to the beam.

The target is filled from the rear via a transfer line from a Philips liquefier. Target full status is determined by the presence of liquid in the intermediate reservoir and by temperature-sensitive level indicators, mounted on the top of each end of the target cell. Target empty status is determined by a similar sensor on the bottom of the cell.

The hydrogen target contains essentially parahydrogen at a pressure of $\sim$ 813 Torr, a temperature of 20.5 °K, and a density of 0.06996 g/cm^3. The density variation due to gas bubbles is calculated to be $\sim 8 \times 10^{-5}$ g/cm^3. The deuterium target is operated at a similar pressure, at a temperature of 23.9 °K and has a density of 0.1614 g/cm^3.

3.2.2 STAC target

The active heavy target[3], called the sampling total absorption calorimeter (STAC), consists of 36 iron/scintillator elements. It has a total iron length of 257 cm and is made up of two sections (see fig. 5). The main section has 26 elements, each 9 cm thick (steps of 2 cm of iron) and 50 × 50 cm^2 in area. The scintillators of each element are viewed by a single EMI 9821 KB photomultiplier. The upstream section[4] consists of 10 elements 40 × 40 cm^2 with a structure different from the main section as shown in fig. 5; Philips 56 AVP photomultipliers are used in this section.

The upstream section and first 20 elements of the main section are used as the target ($\sim$ 1500 g/cm^2). The last six elements, with extra iron plates, are used to absorb hadron showers produced near the end of the target, and to prevent them from penetrating into the forward spectrometer. Four special trigger counters S_1 to S_4 are installed in the STAC for additional trigger conditions, such as defining the beam, during testing and data-taking; in particular, S_4 is used to veto showers leaving the STAC.

The energy resolutions, measured[5] in several test beams, are: $\sigma/E = 0.41/E^{0.4}$ for hadrons and $\sigma/E = 0.22/E^{0.5}$ for electrons. This leads to a resolution $\sigma/E \approx 5.0\%$ for 250 GeV hadrons.

The STAC allows measurement of the energy of the hadronic shower produced by a muon scattering in the target. The comparison of the hadronic shower energy with that lost by the scattered muon can be used to search for "missing energy", which may be produced by weak interactions at the scattering vertex or in the subsequent hadronic shower*). The measurement of the shower length and structure can be used to distinguish between electromagnetic and hadronic showers. In order to measure the large range of pulse heights obtained, between a minimum ionizing particle and a 250 GeV shower, three signals for each photomultiplier are recorded on three separate ADCs: two anode signals (one amplified ten times) and one signal from the third last dynode (20 times smaller). The effects of pulses caused by beam particles not in time with real events are suppressed by the use of small gate width (25 ns) for the ADCs, and by measuring the time of all pulses with TDCs.

Monitoring of the performance and stability of the system is made using non-interacting beam muons and light diodes fired both in and out of the burst. The ADC pedestals are measured once per burst.

3.3 Spectrometer magnet

The forward spectrometer magnet (FSM) is a classical window frame dipole defining a parallelepipedic field volume: 4.30 m along the beam line (x), with a 2 m wide (y) by 1 m high (z) aperture. Two sets of water-cooled copper coils allow a maximum current of 5000 A, corresponding to a power of 1.56 MW. In order

*) The STAC energy resolution, as measured in this comparison and after unfolding the FS contribution to errors, is $\sigma/E = 0.56/E^{0.4}$.

to keep the beam deflection compatible with the downstream experiment (NA4) at different energies, a current of 2000, 4000, or 5000 A has to be used. The magnetic field was measured at these three current values in a total field volume of $6.4(x) \times 1.92(y) \times 0.90(z)$ m^3, using a movable set of Hall probes. Several overlapping rectangular volumes were scanned in steps of 2 cm in x, 6 cm in y and 5 cm in z. Excellent symmetry in x, y, and z was observed. Global fits were made to the data on the surface of the measured boxes. Root mean square deviations of the predicted field values (main component) from the measured values in the volume of the boxes are of the order of 5 G. The estimated fractional accuracy in the measurement of $\int B\, d\ell$ is $< 2 \times 10^{-3}$. The values found are given below:

Current (A)	$\int B\, d\ell$ at $y = z = 0$ (T·m)	Effective length (m)	Saturation from 2000 A (%)
2000	2.328	2.919	-
4000	4.414	2.803	5
5000	5.182	2.734	11

3.4 Hodoscopes and associated electronics

3.4.1 Beam hodoscopes

The beam hodoscopes are fast scintillation counters which measure the beam momentum (BMS), position ($BH_{a,b}$), and intensity (H_5); they do not participate in the electronic trigger.

Momenta of incident muons are measured in the beam momentum station (BMS), which consists of four hodoscope planes located close to the conjugate points of a focusing spectrometer and at intermediate positions; the spectrometer (see fig. 4) is made of the last major vertical bend (24 mrad) of the beam line together with the quadrupole doublets on each side of it. The four planes of horizontal scintillator strips provide an overconstrained measurement of the particle momenta, which is essential in the multiple hit environment resulting from knock-on particles and large beam fluxes.

Each hodoscope is made of up to 64 elements, 5 mm wide, with small overlaps to provide high efficiency. The scintillator strips are divided into several elements in the central region, so that the rate in any element does not exceed 3×10^7/s, even for 10^9 muons/s. As the beam cross-section differs from one plane to another, the element length varies. A thickness of 2 cm is used to obtain a large output signal for good timing.

To enable a reduction of the number of multiple beam tracks, accurate timing of the BMS relative to the detectors of the FS is made. The relative timing of elements within the BMS is adjusted using excited dye-laser light piped to each element by fibre optics[6]. This gives a relative timing of $\lesssim$ 100 ps. A further measurement of this relative timing is made by off-line data analysis; here the timing of each element is made with respect to the mean BMS time using a large sample of clean, single-beam track events. This also achieves a relative timing accuracy of $\sim$ 100 ps. For normal events, the BSM-FS relative timing is determined to $\sim$ 300 ps.

In order to evaluate the beam momentum from the hodoscope information, a Monte Carlo simulation program is used to provide hits on each of the four hodoscope planes with momentum and angles varying over the full beam phase space; a principle component analysis followed by a multidimensional least squares fit results in functional parametrizations of $1/p$, p_y/p_x, and p_z/p_x, plus one test on the compatibility of the four hits. These parametrizations were then used for beam momentum determination. The absolute accuracy, determined by the measured field maps, is estimated to be $\sim \pm 0.5\%$, with a relative accuracy of $\sim \pm 0.3\%$. A check on this was obtained by comparing momenta measured in the BMS and in the FS in a series of runs, carried out at several nominal beam momenta, in which the beam is deflected through the FS chambers.

The two sets of beam position hodoscopes[7], BH_a and BH_b, with 12×12 cm^2 sensitive area, are placed immediately upstream of the target, with a $\sim$ 6 m separation. Each set (see fig. 6) consists of three planes (y,z,θ) of 60 scintillator elements (see table 1). Each element, 0.22 cm wide and 0.4 cm thick, is viewed

by a single 19 mm diameter phototube (EMI 9826A) through a long plexiglas light-guide, bringing bases and shieldings away from the near halo of the beam. A high efficiency (98-100%) over a whole plane is achieved by shifting each second element by 0.45 cm in depth, thus allowing a small overlap ($\sim$ 0.1 mm) of two consecutive elements and resulting in a 2 mm effective spacing. Time resolutions between 300 and 500 ps, depending on the position of the particle along the scintillator, were measured in a pion beam, after rejecting the bad elements. The hodoscopes were tested at high intensity and no significant change in efficiency was found up to 10^8 particles/s on the whole plane.

A special counter (H_5) was designed to give a reliable measurement of the muon beam intensity up to rates of $\sim 4 \times 10^7$ particles/s. It consists of two planes (see table 1) of scintillator elements located at the far end of the experiment behind H_4. The division of the planes in 4 and 5 elements, reduces the rate per element to $< 10^7$/s and the thickness of the elements (1 cm) guarantees good efficiency. Each element is seen by one XP 2020 photomultiplier. The signals of one plane are mixed and the coincidence rates of both planes are recorded. Furthermore, H_5 signals, stretched to 10, 16, and 22 ns, are recorded to allow for dead-time corrections. The hodoscope H_5 is also used to tag the muons which scatter at very small angle with respect to the beam.

Another method to measure the muon flux, which is expected to remain accurate beyond intensities of 10^8 muons/s, is based on the capability of the BMS and BH TDCs to record beam muons which arrive in the 50 ns following the start by a trigger. A random trigger (trigger 10) with accurately known rate is used to start the TDCs. The recorded triggers are then passed through the beam reconstruction and selection software as used for physics triggers, and surviving muon tracks are counted within a window of typically 10 ns (approximately 100 BH TDC counts). Each counted muon represents 1.0/(window width $\times$ random trigger rate) reconstructable beam muons available for physics triggers.

3.4.2 Trigger hodoscopes

Three large hodoscopes H_1, H_3, H_4, together with the veto counters V_1, V_2, V_3, are used to trigger the detection system on a muon scattered in a given region of angle and momentum. H_1 just behind the magnet and H_3 behind the absorber (see fig. 3) define the horizontal and vertical coordinates of the scattered muon at two positions along the beam and therefore the angle of the muon behind the magnet. H_4, at the back of the apparatus, has only horizontal scintillator strips, thus allowing, together with H_3, the determination of the vertical angle component of the muon when it has passed the iron absorber. The element sizes of H_1 and H_3 (see table 1) are determined by the intervals (0.5°) required to adjust the θ cut. The horizontal strips of H_3 and H_4 are divided into two elements to limit the maximum length to 5 m. The elements are arranged in a way to leave a hole of adjustable size for the beam. In front of H_4, a 40 cm thick iron wall, with a hole for the beam, absorbs low-energy electromagnetic showers.

All the elements of H_1, H_3, and H_4 are viewed by two fast (50 mm) photomultipliers through short plexiglas light-guides at each end. The linear pulses feed a splitter-mixer, where groups of eight phototube pulses are mixed and sent to ADCs. The linear signals of each phototube also go into a discriminator (LRS 620CL) set at minimum threshold (30 mV). Since the time differences between both ends of an element are large (35 ns in the case of H_4), mean timers (LRS 624) are used for each element to obtain a signal, the timing of which is independent of the particle position along the scintillator to ±1 ns. These signals are used in the various matrices to form the electronic trigger (see section 4.1). The high voltages of each tube are set to provide full efficiency for minimum ionizing particles crossing the far end of the scintillator. TDCs are connected to one of the hodoscope planes (H_3V) to provide the time correlation (σ = 0.7 ns) relative to the beam hodoscopes.

The veto wall, consisting of a single layer of counters $V_2 + V_3$, is positioned upstream of the target (see fig. 3). An additional layer of counters V_1 is placed between the last elements of the beam line to veto particles at small angles to

the beam which traverse the beam hole of V_2. V_1 is made of four scintillators (see table 1), covering an area of $\sim 130 \times 130$ cm^2 with a square hole for the beam adjustable between 0 and 20 cm in both directions. V_2 is made also of four scintillators covering $\sim 36 \times 36$ cm^2, with a circular hole adjustable from 0 to 20 cm by remote control; this counter defines the accepted beam diameter, which typically is 6 cm. V_3 is made of up to 96 identical counters, assembled with small overlaps, and it covers an area of up to 10×4.5 m^2.

In designing the veto counters and the associated electronics[8] to give high efficiency and acceptable pulse length at rates up to 10 MHz, great care was given to light output and to pulse shaping and discrimination (time-over-threshold discriminators LRS 621 BL/CL). All V_2 and V_3 counters were tested in a pion beam and reached the 10^{-6} inefficiency level for average working voltages of $\sim$ 2000 V. No rate dependence was observed up to a few megaherz and the linear rise of the accidental vetoing with rate was consistent with the measured effective pulse length.

In the experiment, the halo fluxes being more favourable than expected and the maximum beam rates used until now being $\sim 3 \times 10^7$ muons/s, it was possible to reduce the vetoing efficiency requirement on $V_2 + V_3$ with little effect on the trigger rate, by decreasing the high voltage of the counter. The effect of the soft component of the beam (see section 3.1) on V_3 single rates was reduced by erecting a 40 cm thick iron wall just in front of $V_2 + V_3$. In these conditions, the random vetoing at an incident particle rate of 3×10^7/s is $\sim$ 8%. The area covered by V_3 could be reduced to 6×3 m^2, using only $\sim$ 40 counters.

3.5 Proportional and drift chambers

For the reconstruction of the scattered muon and of the hadrons, large drift chambers before (W_1-W_5) and after ($W_{6,7}$) the absorber, and proportional chambers in the beam region (P_0) and inside the FSM (P_1, P_2, P_3) are used.

3.5.1 Beam chambers

The two proportional chambers P_{0a} and P_{0b} [9], both placed between the target and the FSM, are composed of six planes each (2y, 2z, $\theta \pm 30°$). They have

been specially designed to work in beam intensities up to 10^8 muons/pulse. Each plane has 144, 10 μ gold-plated tungsten wires, spaced by 1 mm (see table 2). The wires are soldered on circular printed boards with a control in precision better than ±0.01 mm. A 0.5 mm shift between two consecutive z or y planes results in a 0.5 mm effective wire spacing. A circular frame made of "Stesalit" yields a gap between planes of 3.2 mm. Its diameter of 16 cm makes the use of support wires unnecessary. The cathodes are made of 0.1 mm graphited mylar foils. The chamber is held in place inside a large rectangular frame by 0.5 mm steel wires, thus avoiding heavy material in the FSM acceptance.

Hybrid amplifiers (made by L.M.T.), with a low-input impedance (50 Ω) and a minimum threshold of 1 μA, allow discrimination without dead-time even in pile-ups. They are mounted in a crate placed just outside the FSM acceptance and joined to the wires by 1.5 m long cables made of 50 μ copper strips on a 35 μ thick Kapton support. The signals are then delayed by 120 m of twisted-pair cables with active regeneration at 60 m, followed by receiver modules where the re-formed and differentiated pulses are gated by a strobe derived from the FS trigger, with a 50 ns resolving time.

The wire planes have been selected and tested in order to obtain a 1000 V plateau using an argon-isobutane-freon mixture (see table 2), with 100% efficiency starting at 3600 V. Each plane was accepted when the dark current was less than 1 μA at 4600 V. The high voltage is switched off by a reed relay between each SPS burst in order to quench any discharges and increase the lifetime of the chamber. The planes have been submitted to three weeks' irradiation by a ^{90}Sr source, simulating a 10^8 particles/s beam, without significant loss of efficiency. They have been working in the NA2 experiment at 3.8 kV for nearly two years ($> 10^{13}$ muons) without any sign of deterioration.

3.5.2 Magnet chambers

The three proportional chambers P_1, P_2, P_3, placed within the magnet aperture, have a sensitive area of 180 × 80 cm^2 and each consists of three planes of signal wires: horizontal, vertical, and inclined at 20° to the vertical (see table 2).

The signal wires are of 20 μ diameter gold-plated tungsten, 2 mm apart. The cathode planes, separated by 8 mm from the anode planes, are made from 100 μ diameter beryllium-copper wires, 1 mm apart, stretched horizontally. The wires of both anode and cathode planes are soldered and glued to machined epoxy-glass frames, which maintain an accurate interplane separation. The whole chamber assembly is bolted to two stainless-steel frames for support and rigidity. The signal wire planes are restrained by support lines of PVC-coated beryllium-copper wire every 300 mm to prevent electrostatic instability. A negative voltage of 1.7 kV applied to the support wire reduces considerably the region of insensitivity close to it. The central region of each chamber, where the intense muon beam passes through, is made insensitive by inserting cylindrical enclosures of Kapton, radius 57 mm, between anode and cathode planes[10]. These are glued to the cathode wires and provide a sharply defined insensitive region. The chambers are operated at -5.3 kV using a gas mixture (see table 2) regulated by servo-controlled valves.

The electronics[11] consist of hybrid amplifier-discriminators mounted on the chamber, 100 m of twisted-pair delay cable, and receiver modules which gate and encode the hits from the chamber. The amplifier-discriminator is operated at an input sensitivity of 500 μV into 100 Ω and gives as output a 50 ns wide balanced MECL signal to the twisted pair. At the receiver end the signals are re-formed, differentiated and gated by a strobe derived from the FS trigger, with a resolving time of 75 ns.

3.5.3 Drift chambers

The lever arm in front of the FSM is provided by the drift chambers W_1 and W_2 (1.2 m × 2.2 m) covering the magnet aperture. The back lever arm is made of W_3 (1.2 m × 2.4 m) just behind the FSM and $W_{4,5}$ (2.6 m × 5.2 m) [12,13], 5 m further downstream. Each chamber W_1-W_5 is divided into two modules with independent gas volumes and each module contains four measuring planes (see table 2).

The $W_{6,7}$ chambers, used to identify muon tracks behind the magnetized iron, have to cover a total area of $\sim 4.4 \times 10$ m^2 and are divided in three sections A,

B, and C (see fig. 3 and table 2) of manageable size. Each section is composed of four modules $W_6(1,2)$, $W_7(1,2)$ distributing the coordinate measurements uniformly through the detection volume. This solution has been shown by simulation studies[14] to be more efficient in track-finding in the presence of a large flux of halo muons than the concentration of all measurement in two narrow regions at the front and back of the volume. Sections A and C have 11 measuring planes and section B, where a much higher halo flux is present, has 16 planes. The distribution of measuring planes in all chambers can be seen in table 2.

The drift spaces chosen (see table 2) are compromises between economy of electronics and rate on the individual wires. This rate is essentially due to halo muons in the time acceptance of the chambers, but also to knock-on electrons, particularly in the FSM region. The structure of the drift cells for the different chambers are shown in fig. 7. The sense wires (S) of all drift chambers are made of gold-plated tungsten (Ø 20 μ). All potential wires (P) consist of Cu-Be (Ø 100 μ), except for W_1 where three potential wires (Ø 50 μ) provide an excellent linearity of the space-time relationship. The cathode planes of W_1 to W_5 are made of Cu-Be wires (Ø 50 μ), whereas for $W_{6,7}$ they consist of 3 mm wide Cu strips bonded to 25 mm thick panels with distributed voltages as shown in fig. 8. This design of $W_{6,7}$ follows closely that of a full-size W_6 prototype[15]. W_1-W_7 are supplied with servo-valve (Rotameter) controlled gas mixtures (see table 2).

As beam rates may reach $\sim 5 \times 10^7$ muons/s, it is necessary to desensitize the central region of the drift chambers. For $W_{1,2,3}$ the secondary ionization close to the sense wires is reduced simply by an increase of the wire thickness to 100 μ, in a circular area of 12 cm diameter, by electroplating the sense wire with silver[16]. For $W_{4,5}$, 50 μ polyamide foils[13] are glued on the wires in a central area of 13×14 cm^2. In the central sections (B) of $W_{6,7}$, a region of 18×24 cm^2 is made insensitive by the insertion of small boxes of Kapton[10].

Amplifier-discriminators (CERN types 4241, 4242, 4243) are mounted directly on the chambers and feed their signals via twisted-pair cables to the drift-time recorders (DTR, CERN type 247), which measure the time with a 4 ns resolution.

Mainly due to the amplifiers, the minimum time interval between signals of a single wire is about 60 ns, which corresponds to a minimum track separation of about 3 mm. Test pulses can be fed into the amplifiers to monitor the DTRs and the read-out electronics.

Typical plane efficiencies at a beam intensity of $\sim 10^7$ muon/s range from 93 to 98%, yielding more than 99% efficiency for each chamber package for detecting a track. The space resolutions obtained in the experiment averaging over one plane are: $\sigma \approx 0.3$ mm for W_1-W_5 and $\sigma \approx 0.4$ mm for $W_{6,7}$ [15].

3.6 Particle identification

3.6.1 Čerenkov counter $\check{C}_2$

The threshold gas Čerenkov counter $\check{C}_2$ [17] covers completely the acceptance of the spectrometer magnet and is placed as near as possible behind it, in order to keep its dimensions reasonable (5.30 m wide and 2.40 m high at exit). By filling with neon or with nitrogen at atmospheric pressure, pion/kaon separation can be achieved in the momentum range 20-70 GeV/c or 6-20 GeV/c, respectively.

The length of $\check{C}_2$ is determined by the minimum photoelectron statistics ($N > 5$) necessary for good efficiency with neon ($n - 1 = 0.67 \times 10^{-4}$). A length of 4 m was found to be sufficient provided a high reflectivity of the mirror far into the UV region and a photocathode sensitivity down to 200 nm are obtained.

The mirror is divided into 78 identical spherical ($r = 3$ m) mirrors of 40 cm width and 36 cm height, each focusing the light onto one 125 mm phototube. In fact, the mirrors are in two planes tilted by 20° with respect to the vertical to reflect the light from the particles above the beam plane onto 39 photomultipliers located at the top of the counter and the light from particles below beam plane onto 39 tubes at the bottom (see fig. 8). The spherical mirrors are aluminized, multi-layer, araldite glued assemblies with a reflectivity of the order of 80% for $\lambda \approx 210$ nm.

The dimensions of a cell were chosen to be larger than the Čerenkov light cone for nitrogen ($\phi \approx 21$ cm in the mirror plane) so as to have only one phototube signal per particle in most cases, but also to be small enough to be hit

only by one particle in general. The light spot at the phototube position (at 1.5 m from mirrors) is about 10 cm in the vertical plane but can spread over about 20 cm in the particle bending plane; light funnels of 30 cm entrance diameter are used. The photomultipliers are Philips XP 2041, chosen on the basis of quantum efficiency, cost, and time resolution. Their faces are coated with a thin layer of wavelength shifter, which increases the sensitivity by a factor ~ 2. The anode signals are sent to ADCs (LRS 2249) and pattern units (LRS 2341S). LEDs on the individual channels allow equalization of the ADCs' responses per photoelectron and monitoring of the stability. The efficiency of each cell is then determined from the data, using the ADCs response for scattered muons.

To avoid material in the muon beam and contamination of light produced by beam particles, a 15 cm diameter hole is made in the mirror plane and a black tube (40 μ of Tedlar) with the same diameter runs from one end to the other of C_2.

The large volume of neon involved makes a recycling system necessary. A filter removes impurities, especially oxygen which absorbs light in the UV region.

3.6.2 Calorimeter H_2

The H_2 calorimeter, directly upstream of the absorber, provides some calorimetric ability for neutral particles entering the acceptance of the forward spectrometer as well as a means for the identification of muons, electrons, and hadrons.

The construction of the calorimeter is shown in fig. 9. It is divided into two halves, to the left and right of the beam, and each half is divided longitudinally into three sections. The construction of each half is similar, consisting of sheets of passive high-Z material interleaved with blades of plastic scintillator (Plexipop). The scintillator blades, 1 cm thick, 28 cm wide and 2.8 m long, are grouped together to form forks, each of which is coupled to a single 125 mm photomultiplier (RCA 4522). The attenuation length of the blades is increased to ~ 3 m by placing a yellow filter (Wratten 2E) in front of the photomultiplier. A correction for the residual attenuation is made off line using coefficients determined from a study of the pulse height associated with muons in the beam halo.

The passive material in the upstream module of each half (the "electron" module) is lead and including the steel face plates the total material amounts to 20 radiation lengths (0.95 interaction lengths) and is sufficient to contain an electromagnetic shower in the energy range used. Each such module has two sets of forks, one horizontal set and one vertical set, which are interleaved in the longitudinal direction (see fig. 9). Since one shower is sampled by each view and, within the limits of sampling fluctuations will record an equal pulse height, it is possible to implement some simple pattern recognition of individual electromagnetic showers despite the inherent hodoscope ambiguities. The size of the elements prohibits the resolution of the individual photons from, for instance, π^0 decays.

The downstream modules have only one set of forks each (vertical or horizontal) and the passive material is steel in the form of 4 cm thick plates. No pattern recognition is possible as the sampling is not interleaved. The total thickness of material in the calorimeter is approximately 5.5 interaction lengths.

The energy resolution was measured in a test beam to be: $\sigma/E = 0.4/E^{0.5}$ (GeV) for electrons in the lead module alone, $\sigma/E = 1.5/E^{0.5}$ (GeV) for hadrons in the three modules. These values were checked during analysis of hadrons and electrons in the normal data.

4. ELECTRONIC TRIGGER

4.1 General logic

For the single muon trigger, a scattered muon should fulfil the following requirements:

- target-pointing in both coordinates;
- scattering angle larger than a preselected value;
- momentum larger than a preselected value;
- no hit outside the beam hole in the veto wall.

The block diagram of the basic single muon trigger is shown in fig. 10. The outputs from the mean timers of the hodoscopes H_1 and H_3 are connected to the target-pointing matrices M_0, M_1, M_5. The matrices M_0 and M_1 are used as one large

matrix of size 36 × 50. The two pieces of scintillator composing one element of H_3H or H_4H are connected to one single channel of a matrix. Those channels of H_1V and H_3H which fulfil the target-pointing condition are fed to the angle cut matrix M_2 and momentum cut matrix M_3. With the angle cut matrix the trigger rate is adapted to the $1/Q^4$ behaviour of the cross-section in connection with the available beam intensity. The momentum cut matrix selects muons with momenta larger than $\sim$ 15 GeV/c. It reduces the background from pion decay produced by low-momentum transfer μp interactions. Low-momenta muons are bent vertically out of the acceptance of the matrix by the magnetized hadron absorber, which basically has a horizontal field with opposite directions above and below the beam line. This momentum cut, however, was found to be not very effective, since the horizontal target-pointing has already an intrinsic cut at lower momenta due to the FSM. Therefore, later data have been taken without magnetizing the absorber. For low momenta and small scattering angles, the target-pointing and angle cut matrices can be confused by hadrons or electrons in the hodoscope H_1V. These types of triggers are suppressed by the matrix M_7, which uses hodoscopes H_3H and H_3V. The dead area of this matrix is extended in the direction of the bending of the spectrometer magnet to be effective for lower momenta when the scattering angle is very small.

These requirements together with the veto (V_{1-3}) conditions compose the single muon trigger which is used for liquid H_2/D_2 running. For single-muon measurements with the STAC target, a minimum energy deposit in the target of a few GeV is also required. This threshold is matched to the minimum angle accepted by the angle cut matrix. In addition to the single-arm trigger, a multi-muon trigger is installed. This requires the target-pointing matrices M_0, M_1, M_5, no hit in the veto counters, one hit outside the central channels in H_3H and multiplicities of ≥ 2 in the hodoscopes H_3V and H_4H. For the multiplicity decision in H_3H, a special unit with cluster logic is used. Multi-muon triggers, simulated by large showers leaving the STAC, are strongly reduced by a veto counter at the end of the STAC. This counter rejects events with amplitudes equivalent to more than 20 minimum ionizing particles emerging from the STAC target.

4.2 Trigger rates

The rates for the single-muon trigger, as defined previously, are of the order of 5×10^{-6}/muon for liquid H_2 and 9×10^{-6}/muon for liquid D_2. About 10% of these triggers contain a scattered muon which has effectively fulfilled the trigger conditions. The "false" triggers have several origins. One clear source is high-rate genuine low-angle muon scatters (mostly μe scatters), in which the muon does not satisfy the trigger directly but only with the help of the electron showering, for instance. Such triggers often yield a reconstructed scattered muon ($\sim$ 20% of total rate) which is subsequently removed from analysis by the requirement that it satisfies the trigger itself. The remainder of the false triggers are dominated by rather large hodoscope multiplicities, the easiest way for such a selective trigger system to be confused. Note that the multiplicity in H_4 was reduced by erecting a 40 cm thick iron wall just in front of this hodoscope.

Trigger rates for single muon measurements with the STAC target are typically $\sim 2 \times 10^{-5}$/muon for a 1° angle cut and $\sim 3 \times 10^{-6}$/muon for a 2° cut. The useful content of this trigger is high ($\sim$ 80%), mainly due to the elimination of electromagnetic scatters by the energy deposit requirement in the STAC target itself. The multi-muon trigger has considerably lower rates depending on the particular requirements introduced.

4.3 Trigger matrices

The two-dimensional correlations between the trigger hodoscopes are performed with programmable fast coincidence matrices[18]. To match the channel numbers of the trigger hodoscopes, the size of the matrices was chosen to be 25 × 36. The x and y inputs are twofold with an active OR after the NIM-ECL converters. The x channels for which the coincidence conditions are fulfilled are available on double NIM outputs for use in further decisions. A common OR of all 900 coincidences is available with a high fan-out capability.

The matrices can handle frequencies from d.c. to 125 MHz. The input-output delay is 25 ns for the repeated outputs and 28 ns for the common OR outputs, with a maximum jitter of ±3.5 ns. The programming of the individual channels is performed either by a dual-in-line switchboard or via CAMAC. For both programming

modes the status of each coincidence element is displayed with a light diode. In the experiment, this is performed in the CAMAC mode only. A 900-bit data string is shifted in via a clock and a data line, the output from the last bit of the shift register being available for error detection during the loading procedures. The fast part of the matrix is built in ECL 10000 logic and the programming part in TTL.

5. DATA ACQUISITION

5.1 On-line computer and CAMAC systems

The computer system used (fig. 11a) comprises four PDP-11/70 computers (DAC, U_0, U_1, U_2). The machines are interconnected using five Mbaud serial links via a small PDP-11/10 computer (MUX), which acts as a multiplexer and is also used as a gateway into the CERNET data communications network. This allows access to the CERN computer centre for file storage, program preparation, event reconstruction and collection, and analysis of data samples. Each of the four computers has been connected to CAMAC using a commercially available interface[19]. The interfacing scheme uses the system crate principle, and allows single or multiple computer access to up to four standard, type 4600, CAMAC branches.

The computer labelled DAC is the data acquisition computer. This acquires data, on an event-by-event basis, during the SPS spill. The data is read into a large buffer and then written to magnetic tape. Data acquisition and recording on tape are overlapped during the spill. Outside the spill, the DAC writes any remaining data onto tape and distributes data samples of complete events to monitoring tasks running in the other computers. The other computers are used to monitor both the data and the correct functioning of the apparatus. This is achieved in two ways: by using events supplied on request from the DAC over the computer links and by performing direct hardware checks. Electronics for monitoring and control applications are housed within standard CAMAC. The U_0 computer can directly monitor all equipment attached to the DAC/U_0 shared CAMAC system, including the read-out tree and other conventional CAMAC crates. Nearly all the CAMAC used in the experiment is accessible from both the DAC and the U_0. The U_2

computer, having no direct access to the read-out system, is used almost exclusively to run tasks which monitor the drift and proportional chambers, using event data obtained from the DAC. The U_1 computer is used to run a large photon detector which has recently been added to the forward spectrometer system and will be described in a later publication[20].

In order to achieve the lowest possible dead-time when acquiring data on an event by event basis, extensive use has been made of the CERN developed ROMULUS system[21]. This is a read-only CAMAC based system which allows the acquisition of data from a very large number of CAMAC crates, with a minimum time overhead in setting up a direct memory access transfer into a computer. Figure 11b shows a schematic representation of the configuration used. The read-out is logically divided into a number of distinct sub-branches, each being associated with a piece of apparatus. These sub-branches, which are denoted logical "pieces of equipment" can be enabled or disabled as required via control lines connected to the associated ROMULUS branch driver. An event therefore comprises any combination of the available logical "pieces of equipment". The read-out from equipment located on the upper and lower floors of the control room is collected together before being connected via long-distance branch drivers into the DAC/U_0 CAMAC. Data from the read-out electronics is first buffered in two fast memories before being transferred into the DAC. This allows the electronics to be freed rapidly for subsequent events and also permits a double buffering scheme whereby transfer of event data into the DAC can be overlapped with read-out of the next event. The effective dead-time for acquiring an event of average length 2.5 kbytes is $\sim$ 1.7 ms.

The software falls into two categories: that for data acquisition, and that for monitoring the state of the data and the experiment in general. The data acquisition software is fully described elsewhere[22]. It allows the definition of up to 16 different trigger conditions. A flexible scheme for associating a trigger with the read-out of different parts of the apparatus has been implemented. In addition, any combination of triggers can be written onto any of four different magnetic tape drives. This flexible multi-trigger, multi-magnetic tape mode of

operation permitted the independent setting up and testing of new triggers in parallel with data-taking using well-established triggers. The scheme used for denoting logical "pieces of equipment" has enabled the read-out system to evolve smoothly from the independent testing stage to the final system, without changes to the monitoring tasks' software.

The function of reading the data from CAMAC, writing it out to tape, passing it trigger selectively to monitoring tasks and controlling the operation of the data acquisition system is performed by six tasks and a special "events" module in the RSX-11M system, all written largely in MACRO-11.

5.2 Monitoring the experiment

The currents in the 57 magnetized elements of the muon beam line are automatically checked against reference values by a monitoring program, which requests information via a serial CAMAC-to-CAMAC link from one of the SPS control computers. Beam profiles measured in MWPCs located both upstream and downstream of the apparatus can be displayed via a terminal connected to this computer; this terminal also allows direct access to comprehensive information on the status of the SPS and can be used to initiate hardware tests on the beam momentum hodoscopes.

Each component of the FS has one or more associated pieces of monitoring software which can be initiated manually or at regular time intervals. Most of this software, which is written in FORTRAN, is machine independent and the output is available via a centralized system at any terminal of the computer complex. All status and error messages are displayed on a series of television monitors, printed on a central teletype, and added to a disc-based experiment log.

The use of CAMAC-controlled HV supplies allows the frequent automatic checking of hodoscope and wire-chamber high voltages. The integrity of the electronics from the detectors to the read-out CAMAC can be monitored in a rigorous manner by firing LEDs or injecting test pulses at regular intervals between machine spills; extensive use is also made of the CAMAC initiated test functions available on ADCs, TDCs, etc. Monitoring programs can also accumulate events on a sampling basis, the output normally being in the form of "hit maps", or time- or pulse-height

distributions which can be used to monitor the efficiencies of the detectors or to study event topologies for different trigger conditions. Several simple down-scaled triggers, running in parallel with the main trigger, are used to achieve a uniform illumination of the full apparatus with particle tracks.

All CAMAC and NIM crate voltages, wire-chamber low voltages and some high voltages derived from bulk supplies are checked with a computer-controlled scanner system based on analogue multiplexers and a high-precision digital voltmeter. Overcurrent trips are monitored via TTL status levels connected to a CAMAC register which is checked for fault conditions every few minutes. Simple test programs periodically check the status of the CAMAC system on all four computers; the validity of the word counts and crate markers which are inserted into the event structure by the ROMULUS system is regularly checked for a sample of events and statistics are kept of the different possible types of read-out errors.

Counting rates from the experiment are read out every spill and written onto magnetic tape. Summary tables of raw and normalized rates can be displayed as well as histograms of critical trigger rates and beam intensities as a function of time.

A pictorial representation of particle tracks through the apparatus can be displayed in plane and elevation views and different regions of the equipment viewed in a "blown-up" form. An event can be sent on request to a reconstruction program running in the IBM 370/168 and the reconstructed event can be displayed. Every few hours a sample of a few thousand events is sent to the IBM and accumulated there on disc. The sample is then analysed by a monitoring program, which produces a comprehensive and compact summary of the performance of all detectors in the experiment.

5.3 Data-taking conditions

During data-taking, up to 16 different triggers may run simultaneously. The single-arm trigger is normally running with two different angle cuts: 0.5° and 1°. In addition to the physics triggers, monitoring triggers are running for efficiency measurements and beam-intensity monitoring. There is the possibility to prescale

any particular trigger in order to assign priority to others or avoid prohibitively high dead-times. A maximum of $\sim$ 160 events can be sampled by the DAC during one spill of the SPS and written to tape. The effective spill length, as measured with a delayed coincidence of H_5 with itself, varies from one run period ($\sim$ 10 days) to another, depending on the SPS cycle time (10-12 s). In general, the spill length has been improved from $\sim$ 700 ms in the initial phase of the SPS North Area running (1978) to a maximum of 1800 ms now (1980).

Data are mostly taken at 120, 200, and 280 GeV/c beam momenta, where the muon rates are as given in section 3.1. For liquid targets, primary proton rates per spill of (1-6) $\times$ 10^{12} are used in order to obtain rates of (1-2) $\times$ 10^7 muons/spill. With the trigger rates mentioned in section 4.2, data can usually be accepted without prescaling even the 0.5° trigger, with acquisition dead-times not exceeding 20%. For the STAC target, the used beam intensities were (0.5-2) $\times$ 10^7 muons/spill and the 0.5° trigger was prescaled by up to a factor of 8.

6. OFF-LINE EVENT RECONSTRUCTION

The reconstruction of events in the FS consists of three separate stages: the pattern recognition of muon and hadron tracks using the drift- and proportional-chamber information; geometrical fitting of these tracks to obtain precise determination of momentum, angle, and vertex position; and a "processor" stage, where the information from the subsidiary detectors is treated and condensed. An important step in the reconstruction procedure is the geometrical alignment of the various detector planes; straight line tracks, obtained in special data taken with the FSM switched off, allow the evaluation of small corrections to the surveyor's measurements.

6.1 Pattern recognition and track reconstruction

The first step in the track reconstruction program is the identification of a muon track in the $W_{6,7}$ chambers downstream of the hadron absorber. In this region, the multiplicities of hits recorded in the chambers can be large, since the 6 cm drift cells represent a time window of $\sim$ 1200 ns, making the chambers

more sensitive to halo muons and electromagnetic showers which are produced in the iron absorber especially around the beam hole. The pattern recognition procedure is further complicated by the left-right ambiguities inherent in the drift chambers. Monte Carlo studies[14] showed that the best solution was not to attempt to remove this ambiguity chamber-by-chamber but to reconstruct tracks in each projection (y and z) and use theta information for track association. Most out-of-time tracks do not give a line; those which succeed are rejected by use of information from the hodoscopes. This step is most time-consuming and if no muon track is found the event is dropped.

Once a muon track has been found in $W_{6,7}$ it is extrapolated, allowing for multiple scattering, through the absorber to $W_{4,5}$ and W_3 where a search for tracks is made, also using projections. A simple parametrization of the magnetic field is used to continue the search upstream of the magnet and associate points in $P_{1,2,3}$ and $W_{1,2}$ or P_0. Once a muon track has been successfully found, a search starting from $W_{4,5}$ is made for hadron tracks. At this point, all track candidates have been found and a vector of y, z, and θ plane hits for each line, together with the raw data of the event, is written to an intermediate magnetic tape.

6.2 Geometrical event reconstruction

The geometry program performs track and vertex fits to establish the event topologies and kinematics. Tracks are fitted in two orthogonal projections (xy and xz) using the "Quintic Spline" method[23]. This allows a variable number of y and z points in projections or space points. The effects of multiple scattering are included for tracks of less than 100 GeV/c momentum. Of fundamental importance to the momentum determination is an accurate representation of the field in the FSM. This was measured as described in section 3.3 and the three field components were parametrized as even or odd local polynomials in z at optimized x and y values, using quadratic interpolation in the x and y dimensions. For a r.m.s. difference between the polynomial and global representation of $\sim$ 2 G, 10,000 words of storage were required for the polynomial coefficients.

The input to the program consists of the vectors of points associated with a track by the reconstruction program. Beam tracks are fitted as straight lines in the beam hodoscopes; muon and hadron tracks are fitted as far as $W_{4,5}$ by firstly reducing all data from each chamber package to y or z points, there being no advantage to using angle plus point fits since the chambers are situated in field-free regions. Three-dimensional line fits, projection fits, or single points at the y or z planes are used as input to the line fits depending upon the information available from each chamber package. An iterative procedure is then used to reject points inconsistent with the parameters of the track fit and the track refitted, starting with line fits in each detector. A simple helix model, which includes energy loss and multiple scattering, is used to track muons through the absorber and a χ^2 is constructed, which indicates the quality of the link with the line fit of $W_{6,7}$.

Vertices are fitted using the single-track fits as input; Lagrangian multipliers are used in order to force a common vertex constraint in the minimization of χ^2 on the track slopes and intercepts. The track parameters are improved in the constraint fit. In order to obtain muon vertices unbiased by hadrons and avoid the effect of secondary interactions, all like-sign muon-muon vertices are found (and the parameters retained) before any attempt is made to fit hadron tracks to them. Hadron vertices are then fitted by including hadron tracks which pass within a minimum normalized distance of closest approach to a like-sign muon vertex. Opposite sign muon vertices, V_0 vertices, and the highest multiplicity vertex of any remaining hadron tracks (to look for hadron interactions in the target) are then fitted. Any tracks which were found only in W_3 or $W_{4,5}$ are fitted to the vertices already found.

The output of this programme is again an intermediate Data Summary Tape (so-called MAXI DST) which contains fitted track and vertex parameters, the line vectors from the reconstruction program, and the raw event data. At this point, there is the maximum geometrical and kinematic information available which, together with the raw event data, is used as input to the "processor" stage of the

analysis chain. In addition, the reconstruction and the geometry programs may be re-run from this MAXI DST in order to make specific studies.

6.3 "Processor" stage and "MINI DST"

Once an event has been reconstructed and its topology and kinematics established, there still remains a large amount of information associated with other detectors, such as the STAC target, the H_2 calorimeter and the Čerenkov counter $\check{C}_2$, which must be interpreted. Usually, it is necessary to use high-quality track information in order to do this; charged particle identification is attempted using H_2 and $\check{C}_2$; the reconstructed scattered muon is tested to see if it fulfils the hardware trigger condition; a search is performed for tracks seen only in the chambers upstream of the magnet, and so on. In addition, there are independent "processors" which attempt the recognition of electromagnetic showers in H_2, study the beam phase space and normalization, etc. At this stage, it is possible to make selections on the events and write the data in a condensed form to a MINI DST. A compression of about 20:1 between the raw data tapes and the final DSTs is achieved without kinematic or trigger cuts.

The data written to the MINI DSTs include the entire set of kinematic parameters for an event as well as sufficient extra information to allow high-statistics studies of detector performance to be made, for instance, the study of plane efficiencies. Also included, in special records, is normalization information. The DSTs are read with a simple program which allows histograms to be accumulated and manipulated with the HBOOK[24] facility to permit easy physics output. This program may also be used to write selected DSTs and read pseudo-DSTs written by the Monte Carlo program for data with Monte Carlo comparison.

6.4 Experimental resolutions

Resolutions in the drift chambers W_1-W_7, as they appear to be after reconstruction by the geometry program, range from 0.3 to 0.7 mm owing to contributions from small non-linearities in the space-time relations and from small irregularities in the wire positioning. The momentum resolution obtained for a secondary track of momentum p (GeV/c) is then: $\sigma(p)/p \approx (14 + 0.73\ p + 240/p) \times 10^{-4}$ for

280 GeV muons on a liquid H_2 target. At 120 GeV, the resolution is larger owing to the use of a lower field: $\sigma(p)/p \approx (48 + 1.76\ p + 83/p) \times 10^{-4}$. The observed angular resolutions in both planes vary from 0.1 to 0.6 mrad, depending on the momentum of the particle and on the position of the interaction in the target. The vertex is determined with resolutions $\sigma y \approx \sigma z \approx 0.7$ mm and $\sigma x(\text{mm}) \approx$ $\approx (0.85 + 15/p)/\theta$ for liquid H_2 or D_2.

For the STAC target, the momentum resolution is of the same order as for liquid targets, but vertex and angle resolutions are considerably enlarged by multiple scattering in the iron traversed by the secondaries.

Figure 13 shows a dimuon mass spectrum obtained with 280 GeV muons and the liquid D_2 target; a J/ψ peak with a mass resolution of $\sigma \approx 35$ MeV and a peak position of (3.089 ± 0.004) GeV is observed. The mass resolution expected from momentum and angle resolutions including multiple scattering in the 6 m target is $\sigma \approx 25$ MeV. The displacement with respect to the known J/ψ position is $\lesssim 0.3\%$.

7. CONCLUSION

The operation of the spectrometer for nearly two years has shown a high degree of reliability of all detectors, of the electronics, and of the data-acquisition system. A large amount of data on inelastic muon scattering on liquid H_2, on liquid D_2 and on the STAC target, at several energies, is being collected and analysed. Some results are published[25-28].

At present, data are taken with a lead-glass photon detector integrated in the forward spectrometer. This additional detector will be described in a separate publication[20]. A 0.8 m polarized butanol target is being prepared for measurement of the spin-dependent structure functions. Also a large vertex detector system[29] is being built and will be installed during the long SPS shutdown. Based on a large streamer chamber inside a dipole magnet complemented by Čerenkov counters, and time-of-flight and position detectors, it will extend the range of detection of charged hadrons into the backward c.m. hemisphere of the photon-nucleon system (experiment NA9).

Acknowledgements

We are grateful to a large number of people who have been involved in the construction and operation of this experiment. We wish to thank in particular:

- all the technical and engineering staff of the home laboratories, who contributed to the design, construction, and maintenance of the detectors;
- the SPS Experimental Area group for providing us with the high-intensity muon beam and its facilities;
- the SPS accelerator group for the steadily improved running of the SPS and the North Area extraction;
- the SPS survey group for the difficult task of surveying with precision so many large detectors;
- the CERN target group for the efficient running of the liquid H_2 and D_2 targets;
- the SPS EHN2 crew for continuous help during installation and maintenance;
- G. Juban for his constant assistance in the technical maintenance;

  A. Mazzari for her secretarial work and important help in organizing the collaboration, and together with Y. Camp for invaluable work in data handling.

REFERENCES

1) European Muon Collaboration, Proposal SPSC/P-18, CERN/SPSC/74-78 (July 1974), ("White book").

2) R. Clifft et al., The CERN SPS muon beam line, to be published.

3) W. Flauger et al., A heavy iron sandwich target for deep inelastic high-energy muon scattering experiments, to be published.

4) V. Korbel, Thesis, Hamburg, 1972.

5) V. Korbel et al., Calibration tests of the heavy target STAC, Report EMC 77/48, (1977).

6) D. Brahy and E. Rossa, Nucl. Instrum. Methods 158 (1979) 121.

7) J.J. Aubert et al., Nucl. Instrum. Methods 159 (1979) 47.

8) R. Mount et al., Nucl. Instrum. Methods 160 (1979) 23.

9) J.C. Thénard et al., High performance proportional chambers for very intense beams, to be published.

10) M. Edwards et al., to be published.

11) D.J. White, Rutherford Lab. report RL-78-023 (1978).

12) F.W. Brasse et al., DESY report F21-76/02 (1976).

13) F.W. Brasse et al., to be published.

14) C. Besson, 3rd cycle thesis, Grenoble (1976).

15) K.A. Connel et al., Nucl. Instrum. Methods 144 (1977) 453.

16) U. Hahn et al., Nucl. Instrum. Methods 156 (1978) 211.

17) J.J. Aubert et al., A large multicell threshold gas Cerenkov counter, submitted to Nucl. Instrum. Methods.

18) W. Flauger et al., A fast programmable matrix coincidence system, to be published.

19) GEC-Elliott system.

20) J.C. Thompson et al., A high resolution high-energy photon detector, to be published.

21) P.J. Ponting, A guide to ROMULUS/REMUS data acquisition systems, EP electronics, Note 80-01 (Feb. 1980).

22) D. Botterill et al., Nucl. Instrum. Methods 166 (1979) 541.

23) H. Wind, Nucl. Instrum. Methods 115 (1974) 431.

24) HBOOK, CERN computer library routine.

25) European Muon Collaboration, Phys. Lett. 89B (1980) 267.

26) European Muon Collaboration, A study of dimuon events in 280 GeV muon interactions, preprint CERN-EP/80-61 (1980) and submitted to Phys. Letters.

27) European Muon Collaboration, A study of trimuon events in 280 GeV muon interactions, preprint CERN-EP/80-62 (1980) and submitted to Phys. Letters.

28) European Muon Collaboration, Inelastic J/ψ production in 280 GeV muon-iron interactions, preprint CERN-EP/80-84 (1980) and submitted to Phys. Letters.

29) European Muon Collaboration, A study of final states in deep inelastic lepton scattering by the addition of a vertex detector, SPSC/P-18/Add.1, CERN/SPSC/77-113 (1977).

Table 1

Main parameters of the counters

Equipment	Position a) x (m)	No. of planes	No. of elements per plane	Scintillator thickness (cm)	Dimensions of one element y × z (cm^2)	Total area per plane y × z (cm^2)	Beam size hole y × z (cm^2)	No. of phototubes per element	Phototube	
									Type	Diameter (mm)
BMS	-170/-80	4	64	2.0	(10-60) × 0.5	120 × 100	-	1	EMI 9826B RTC 1910	13
$BH_{a/b}$	-16.5/-10.5	3/3 (y,z,20°)	60	0.4	12.0 × 0.22	12.0 × 12.0	-	1	EMI 9826A	19
V_1	∿ -30	1	4	1.0	70 × 70	120 × 120 (min.)	(0-20) × (0-20)	1	XP 2020	50
V_2	-11.7	1	4	0.5	25 × 25	30 × 30 (min.)	Ø 0-20 cm	2	XP 2020	50
V_3	-11.3	1	≤ 96	2.0	50 × 100	1000 × 450 (max.)	35 × 35	1	EMI 9813KB	50
H_1H	2.5	1	18	0.5	250 × 7	250 × 125	14 × 14	2	EMI 9813KB	50
H_1V	2.7	1	36	1.0	7 × 130	250 × 130	14 × 14	2		
H_2	8.7-10.2	3 sections	40/20/20 forks per section	1.0	280 × 28 (1 fork)	560 × 280	Ø 20 cm	1	RCA 4522	125
H_3H	12.5	1	2 × 23	2.0	390 × 15	765 × 345	18 × 15	2	EMI 9813KB	50
H_3V	12.8	1	50	2.0	15 × 340	750 × 340	15 × 18	2	XP 2020	50
H_4H	18.5	1	2 × 29	2.0	500 × 15	996 × 430	26 × 15	2	EMI 9813KB	50
H_5	19.0	2	4/5	1.0	(1-8) × 20	19 × 20	-	1	XP 2020	50
C_2	3.0-7.6	1	78 cells	-	40 × 36 mirror	530 × 240 (exit)	Ø 15 cm	1	XP 2041	125

a) x = 0 at middle of FSM.

Table 2

Main parameters of the wire chambers

Wire chamber	Sensitive area z × y (m^2)	Plane structure	Wire or drift space (mm)	Drift velocity (mm/ns)	Anode-cathode gap (mm)	Gas mixture (%)					
						Argon	Isobutane	Methane	Ethane	Freon	Methylal
P_{0a}	Ø 14.4 cm	$\theta^-,z,z,y,y,\theta^+$	1	-	3.2	75	25			1	
P_{0b}	Ø 14.4 cm	$\theta^-,z,z,y,y,\theta^+$ $\theta^{\pm} = \pm 30°/y$	1	-	3.2	75	25			1	
P_1	0.8 × 1.8	z,y,θ	2	-	8	71.5	23.8			0.7	4.0
P_2	0.8 × 1.8	θ,y,z	2	-	8	71.5	23.8			0.7	4.0
P_3	0.8 × 1.8	θ,y,z $\theta = 20°/y$	2	-	8	71.5	23.8			0.7	4.0
W_1	1.2 × 2.2	$\theta^{-\prime},y',\theta^{+\prime},z',\theta^-,y,\theta^+,z$	10	0.053	6	81.5	1.5	17			
W_2	1.2 × 2.2	$z,\theta^-,y,\theta^+,\theta^{-\prime},y',\theta^{+\prime},z'$	10	0.053	6	81.5	1.5	17			
W_3	1.2 × 2.4	$z,\theta^-,y,\theta^+,\theta^{-\prime},y',\theta^{+\prime},z'$ $\theta^{\pm} = \pm 30°/y$	10	0.053	6	81.5	1.5	17			
W_4	2.6 × 5.3	$yy',z'z,\theta^-\theta^{-\prime},y'y$	20	0.050	10	77	2	21			
W_5	2.6 × 5.3	$zz',\theta^-\theta^{-\prime},yy',z'z$ $\theta^- = -30°/y$	20	0.050	10	77	2	21			
W_6 A	3.48 × 2.88	$zy\theta^-,z'y'\theta^-$	60	0.051	7.5	65			35		
B	3.48 × 2.88	$zy\theta^-z'y',zy\theta^-$	60								
C	3.48 × 2.88	$zy\theta^-,z'y'\theta^-$	60								
W_7 A	4.32 × 3.48	$zy,z'y'\theta^-$	60	0.051	7.5	65			35		
B	4.32 × 3.48	$zy\theta^-,z'y'\theta^-z''y''$	60								
C	4.32 × 3.48	$zy,z'y'\theta^-$ $\theta^- = -60°/y$	60								

Figure captions

Fig. 1 : Kinematics (Q^2-ν plot) of muon-nucleon scattering at E = 280 GeV. Lines of constant W (recoil hadron mass), θ (muon angle of scatter), and x (Bjorken scaling variable) are shown.

Fig. 2 : Artist's view of the forward spectrometer. BH are beam hodoscopes, V_{1-3} are veto hodoscopes, P_{0-3} are multiwire proportional chambers, W_{1-7} are drift chambers, $H_{1,3,4}$ are scintillator hodoscopes, H_2 is the calorimeter and $\check{C}_2$ is the Čerenkov counter.

Fig. 3 : Plan view of the apparatus. The labelling is the same as in Fig. 2.

Fig. 4 : Structure of the muon beam line, EPB is the ejected proton beam and T_6 the primary target; BH and BV are horizontal and vertical bending magnets; HA is the hadron absorber; CMH and CMV are the horizontal and vertical magnetic collimators; BMS is the beam momentum station and EHN2 is the experimental hall number 2 of the SPS North Area.

Fig. 5 : Structure of the STAC target; S are scintillators, S_{1-4} are special scintillation counters which may be used in the trigger.

Fig. 6 : Photograph of one of the beam position hodoscopes.

Fig. 7 : Drift cells of the chambers W_{1-7}; S and P are sense wires and potential wires. All distances are in mm.

Fig. 8 : Side view and optics of the Čerenkov $\check{C}_2$.

Fig. 9 : Structure of the H_2 calorimeter. The lower part shows details of the electron module (1).

Fig. 10 : Trigger logic diagram. The convention about matrix use is that a signal taken from near one corner (e.g. $M_{2,3,7}$) is a common OR from all coincidences satisfying the matrix conditions. In other cases ($M_{0,1,5}$) the signals arriving at the top are passed on individually for further use, if the specific matrix condition is satisfied. The shaded areas represent regions of selected coincidence.

Fig. 11 : Data-taking configuration for computers and CAMAC; U_0, U_1, U_2 and DAC are PDP11/70 computers; MUX is a PDP11/10.

Fig. 12 : The read-out tree. The key is:

ROCC = ROMULUS crate controller,

ROBD = ROMULUS branch driver,

ROOT = ROMULUS branch driver at root of tree,

DRV = long distance driver for ROMULUS branch,

RBUF = 8 kbyte ROMULUS buffer module,

DOWN = ROBD driving downstairs part of read-out tree,

UP = ROBD driving upstairs part of read-out tree.

The CAMAC modules in the two bottom crates are ROBDs or ROBD compatible units driving sub-branches of the read-out tree.

Fig. 13 : Mass spectrum of muon pairs showing J/ψ production by 280 GeV muons on the liquid-D_2 target.

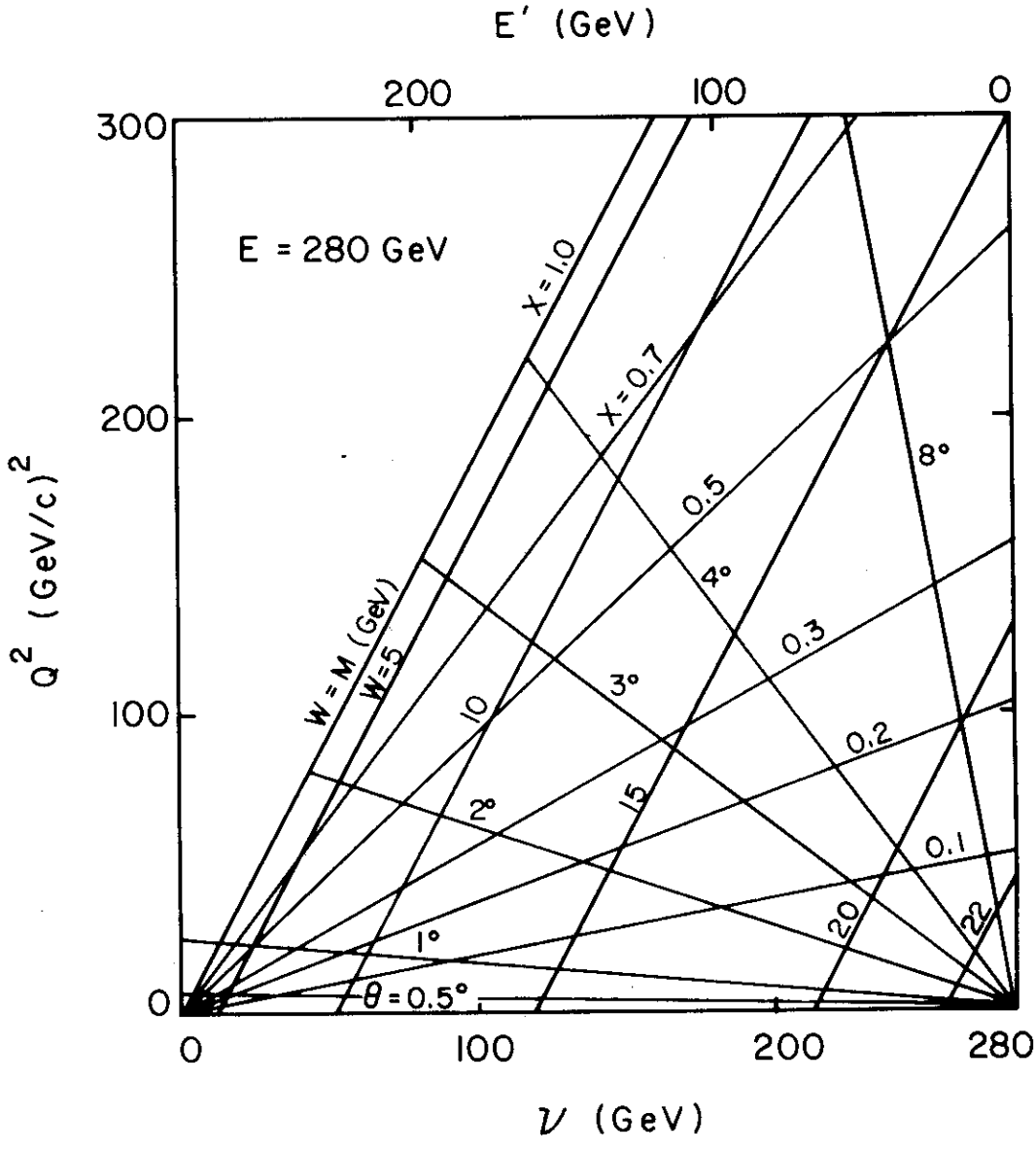
E' (GeV)
200
100
0
300
200
100
0
E = 280 GeV
X=1.0
X=0.7
0.5
8°
4°
0.3
3°
10
W=5
W = M (GeV)
2°
15
0.2
0.1
20
22
1°
θ = 0.5°
Q^2 (GeV/c)^2
0
100
200
280
ν (GeV)

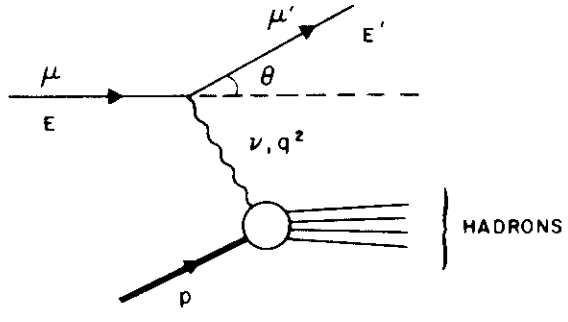
μ'
E'
μ
θ
E
ν, q²
HADRONS
p

Fig. 1

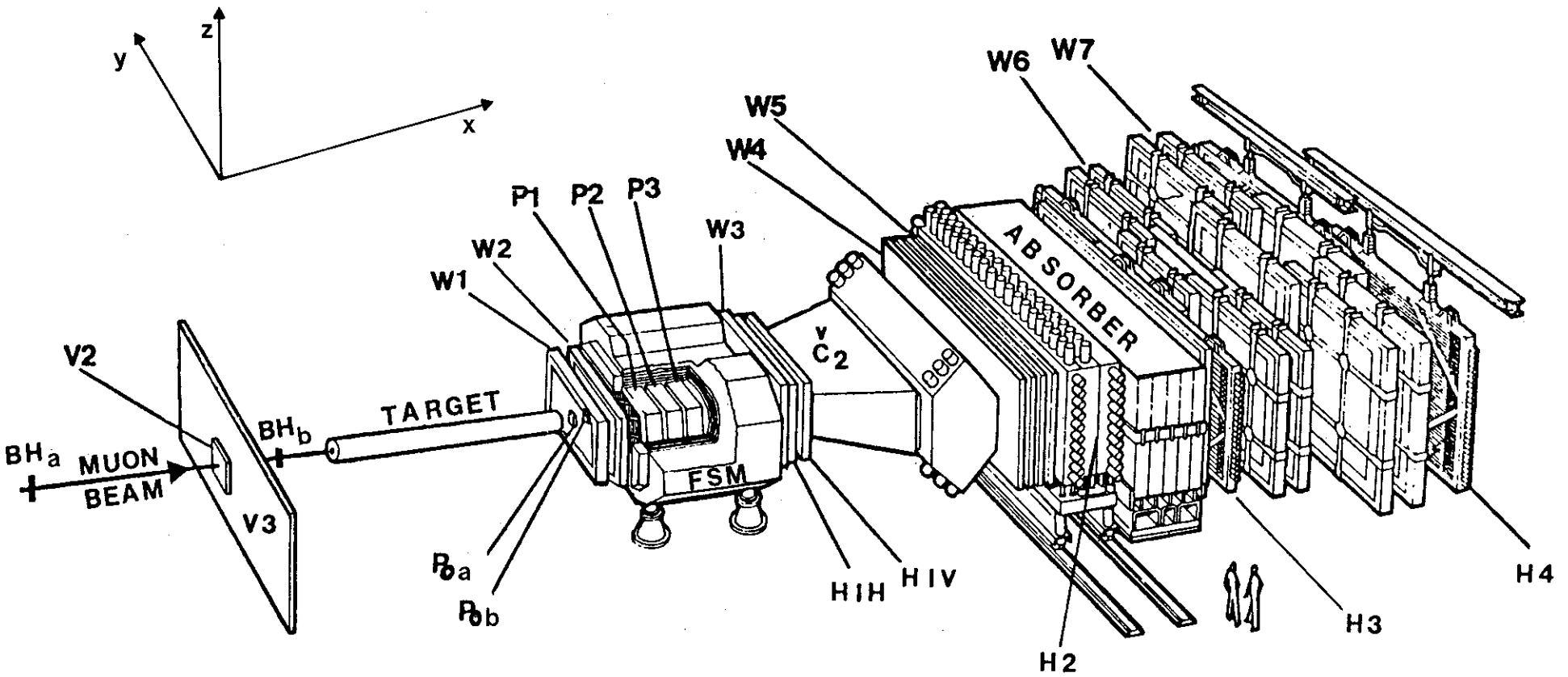
z
y
x
W6
W7
W5
W4
P1
P2
P3
W3
W2
W1
ABSORBER
V2
C_2
TARGET
BH_b
BH_a
MUON
BEAM
V3
FSM
P_{0a}
P_{0b}
H1H
H1V
H2
H3
H4

Fig. 2

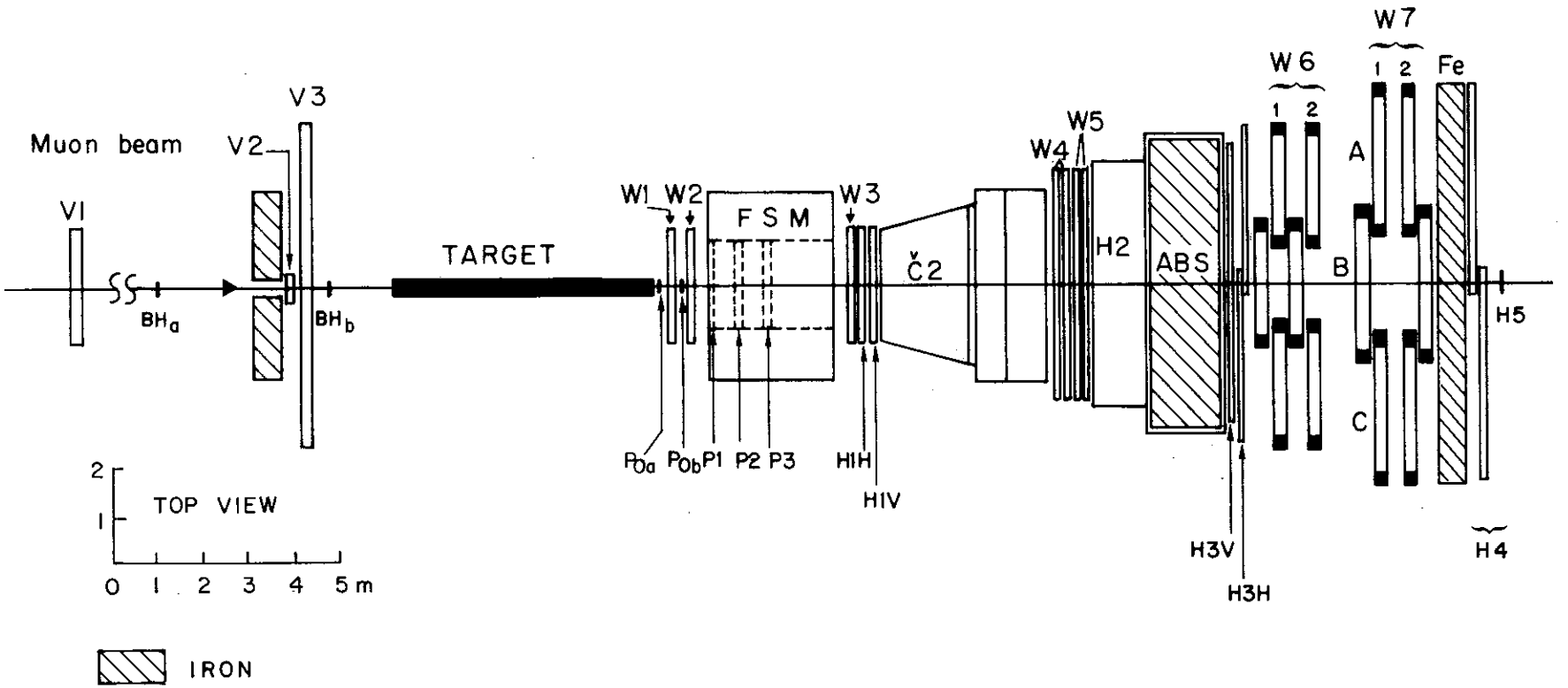
Muon beam
V1
V2
V3
BHa
BHb
TARGET
W1
W2
FSM
W3
C2
W4
W5
H2
ABS
W6
1
2
W7
1
2
Fe
A
B
C
H5
H4
H3V
H3H
H1H
H1V
P0a
P0b
P1
P2
P3
TOP VIEW
2
1
0 1 2 3 4 5 m
IRON

Fig. 3

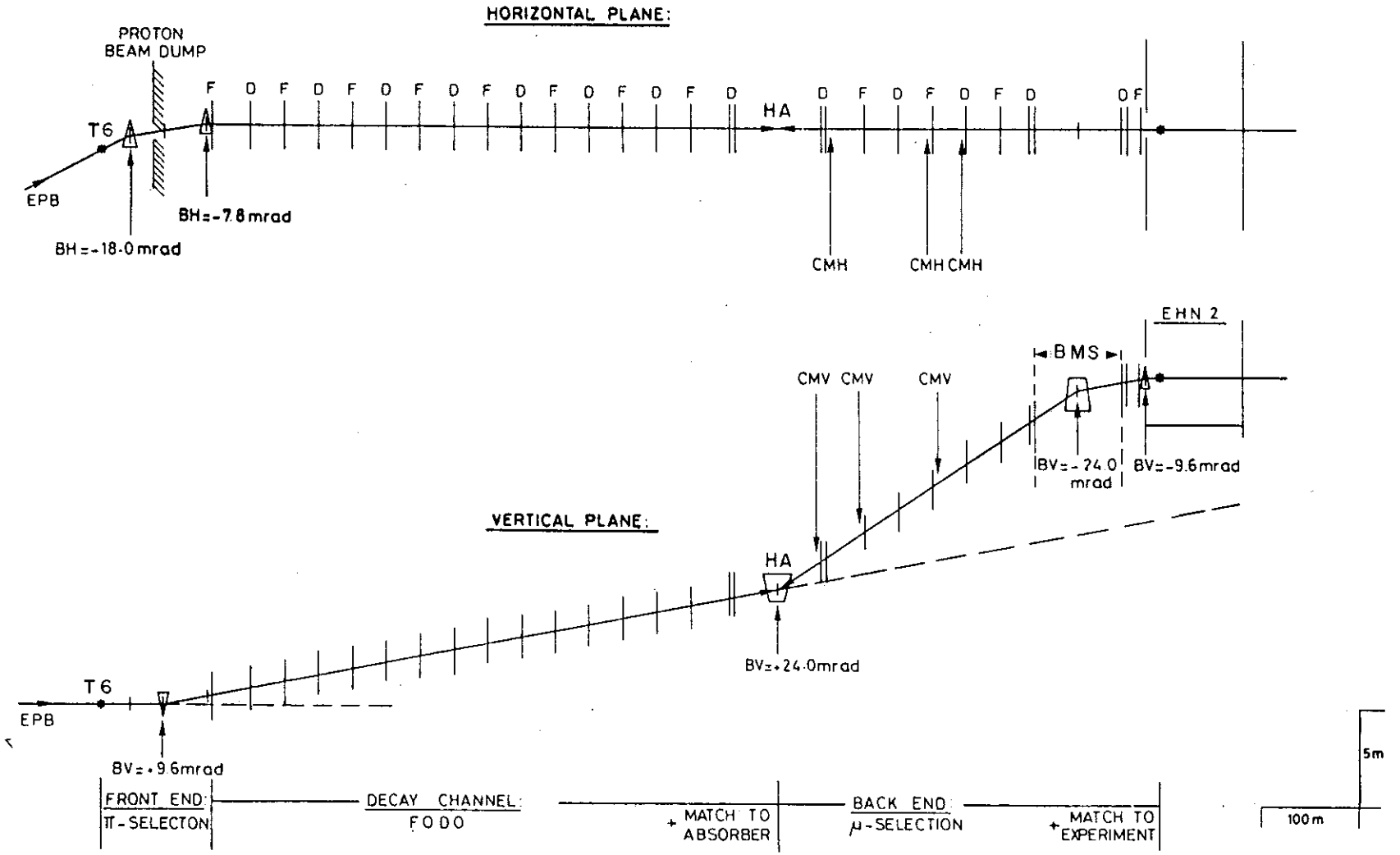
HORIZONTAL PLANE:
PROTON BEAM DUMP
T6
EPB
BH=-18.0 mrad
BH=-7.8 mrad
F D F D F D F D F D F D F D F D
HA
D F D F D F D
CMH
CMH CMH
O F
EHN 2
BMS
CMV CMV
CMV
BV=-24.0 mrad
BV=-9.6 mrad
VERTICAL PLANE:
HA
BV=+24.0 mrad
T6
EPB
BV=+9.6 mrad
5m
100 m
FRONT END:
π-SELECTON
DECAY CHANNEL:
FODO
MATCH TO ABSORBER
BACK END:
μ-SELECTION
MATCH TO EXPERIMENT

Fig. 4

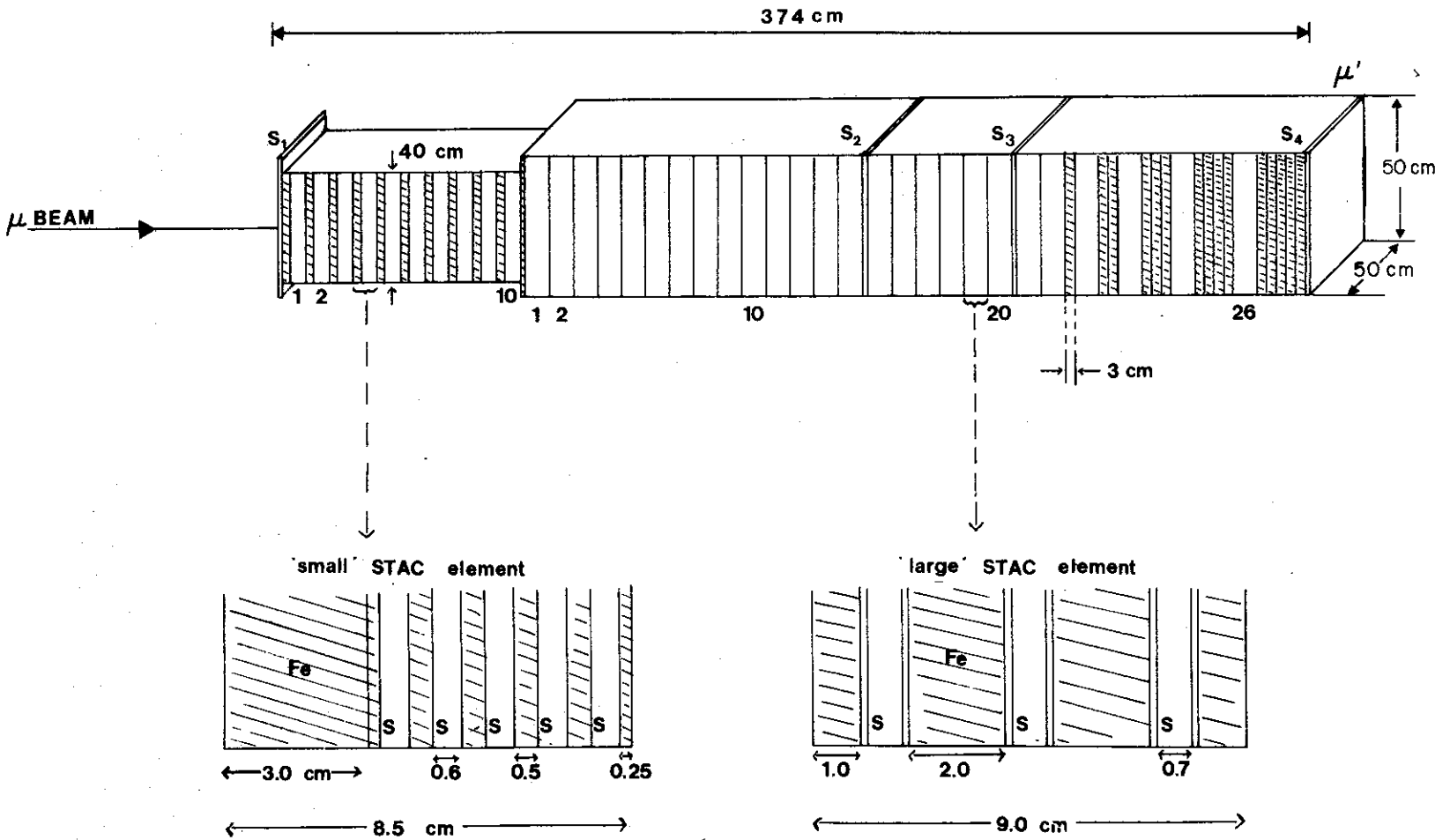
374 cm
μ'
S1
40 cm
S2
S3
S4
50 cm
μ BEAM
50 cm
1 2
10
1 2
10
20
26
3 cm
'small' STAC element
'large' STAC element
Fe
S
3.0 cm
0.6
0.5
0.25
8.5 cm
1.0
2.0
0.7
9.0 cm

Fig. 5

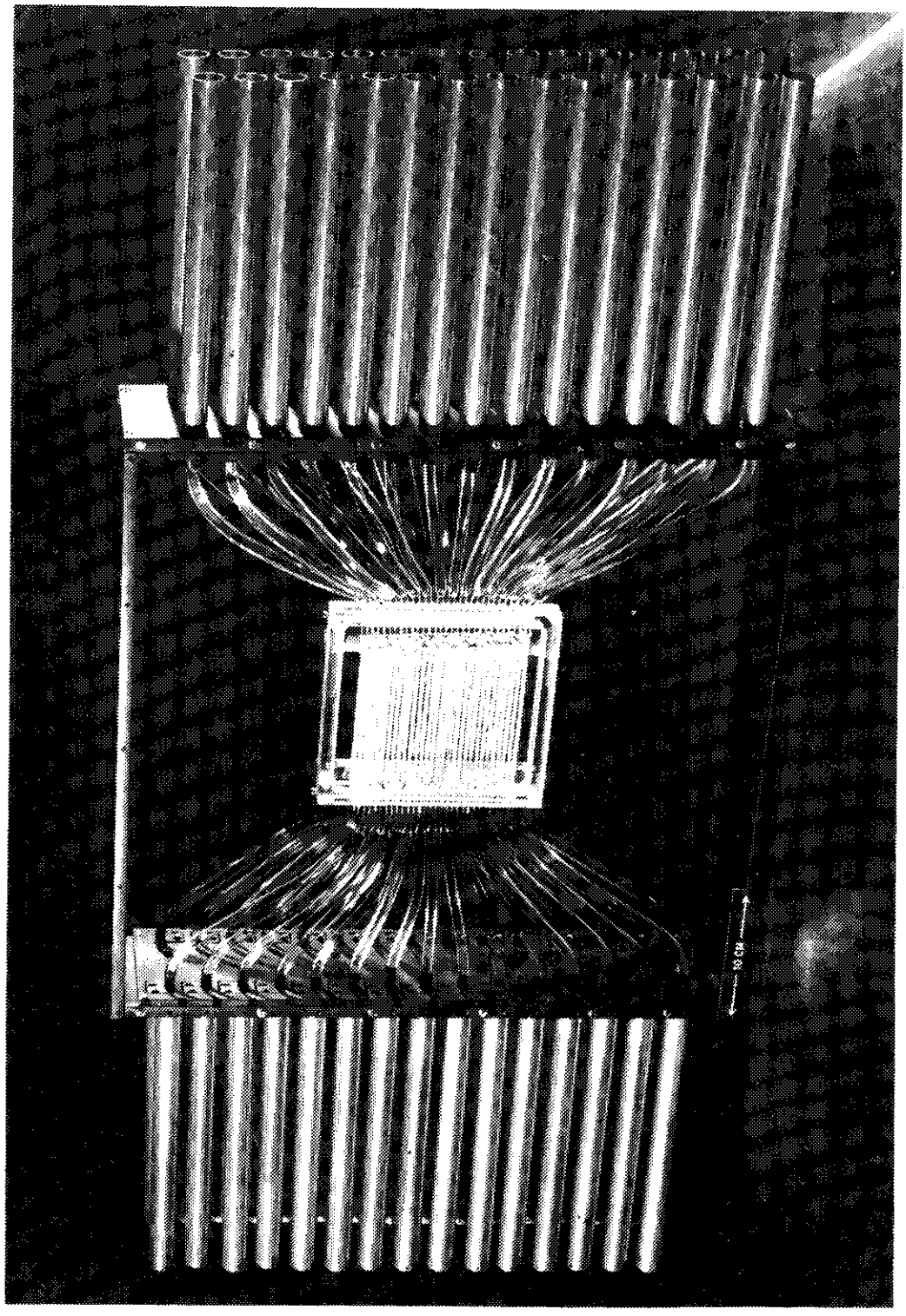

Fig. 6

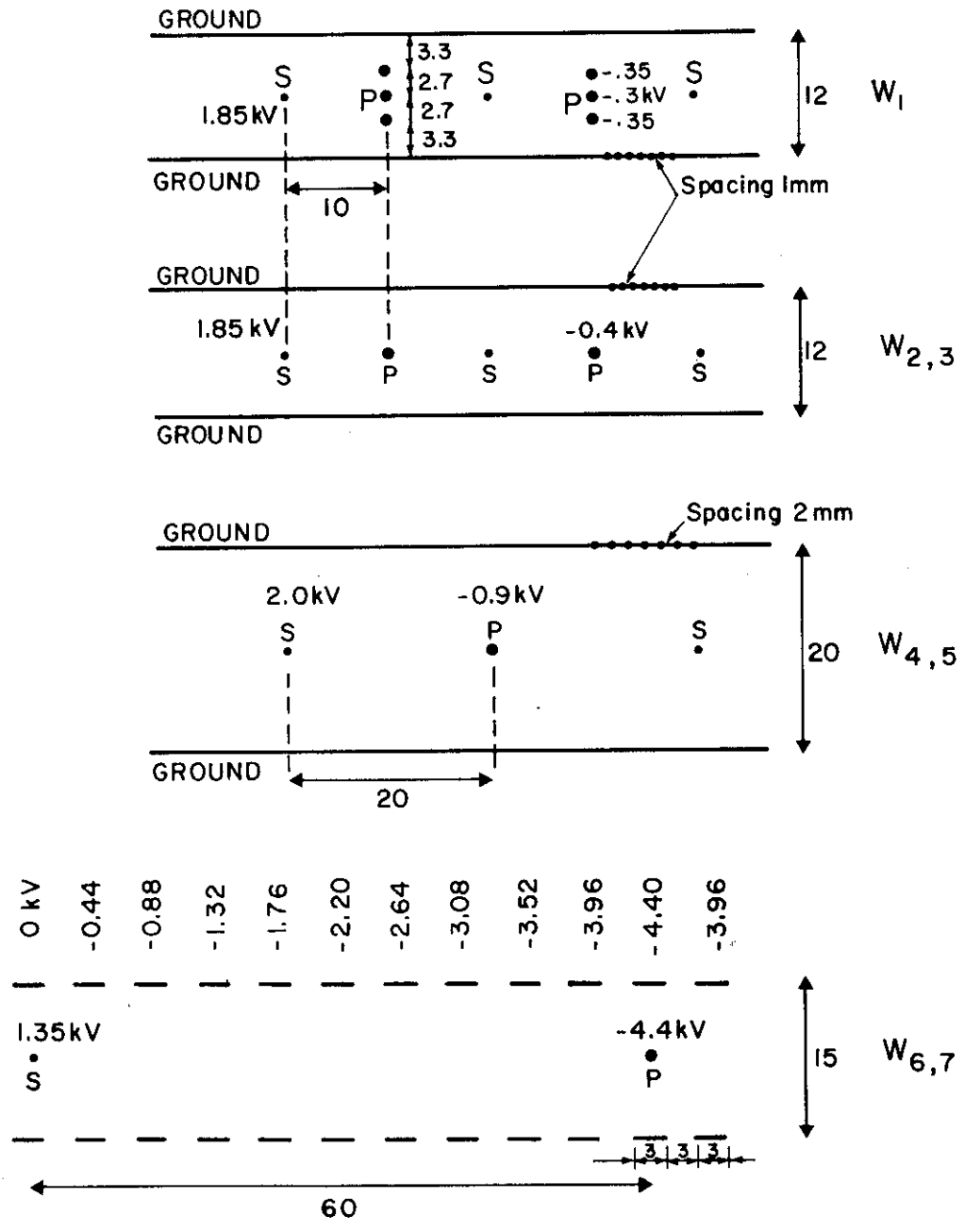

All distances in mm

Fig. 7

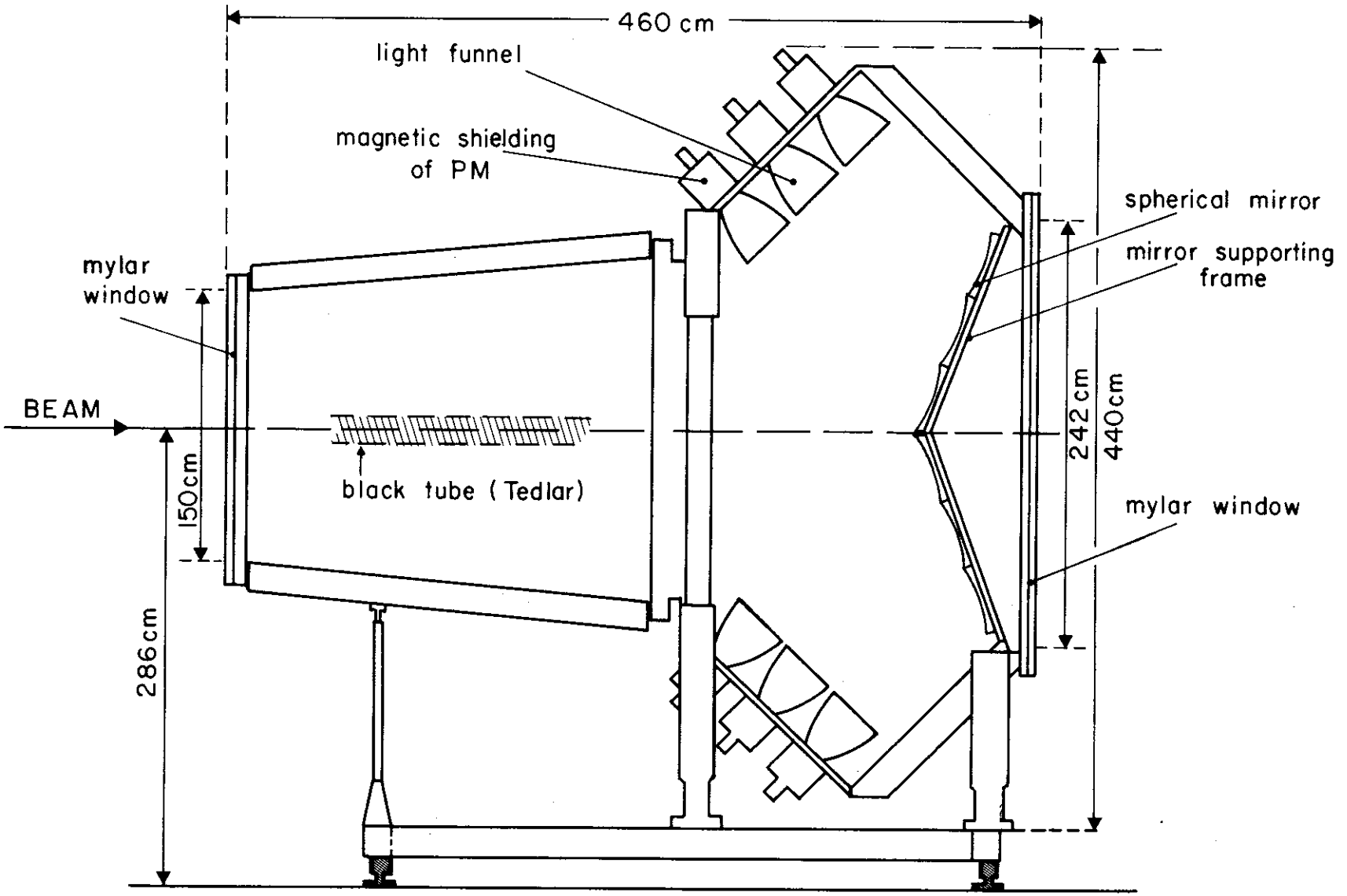
460 cm
light funnel
magnetic shielding
of PM
spherical mirror
mirror supporting
frame
mylar
window
BEAM
242 cm
440cm
150cm
black tube (Tedlar)
mylar window
286cm

Fig. 8

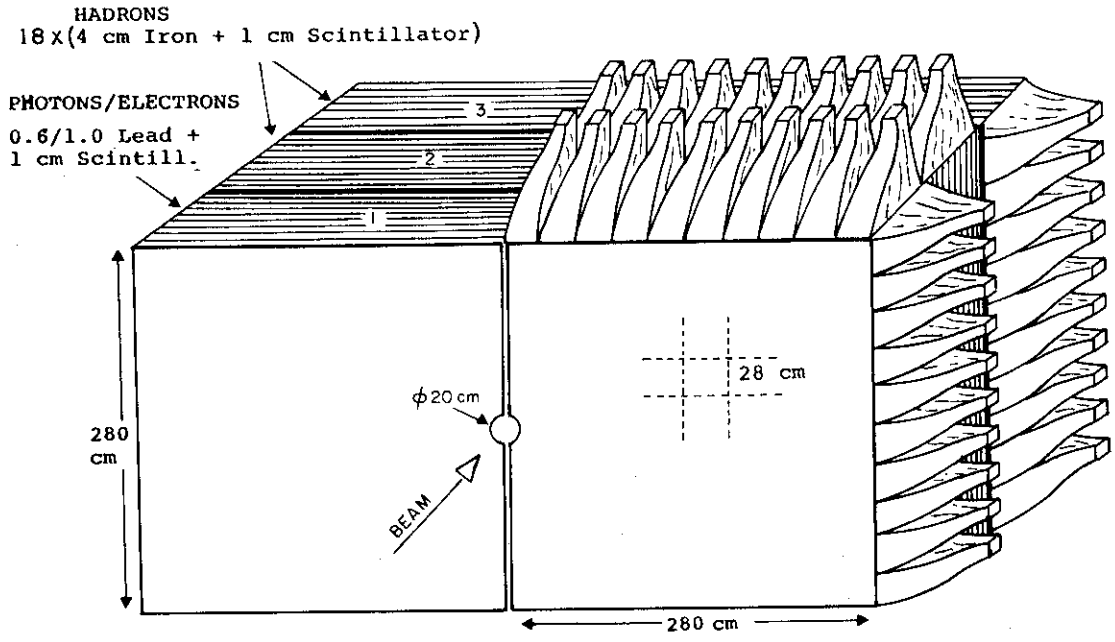
HADRONS
18 X(4 cm Iron + 1 cm Scintillator)
PHOTONS/ELECTRONS
0.6/1.0 Lead +
1 cm Scintill.
3
2
1
280
cm
φ20 cm
BEAM
28 cm
280 cm

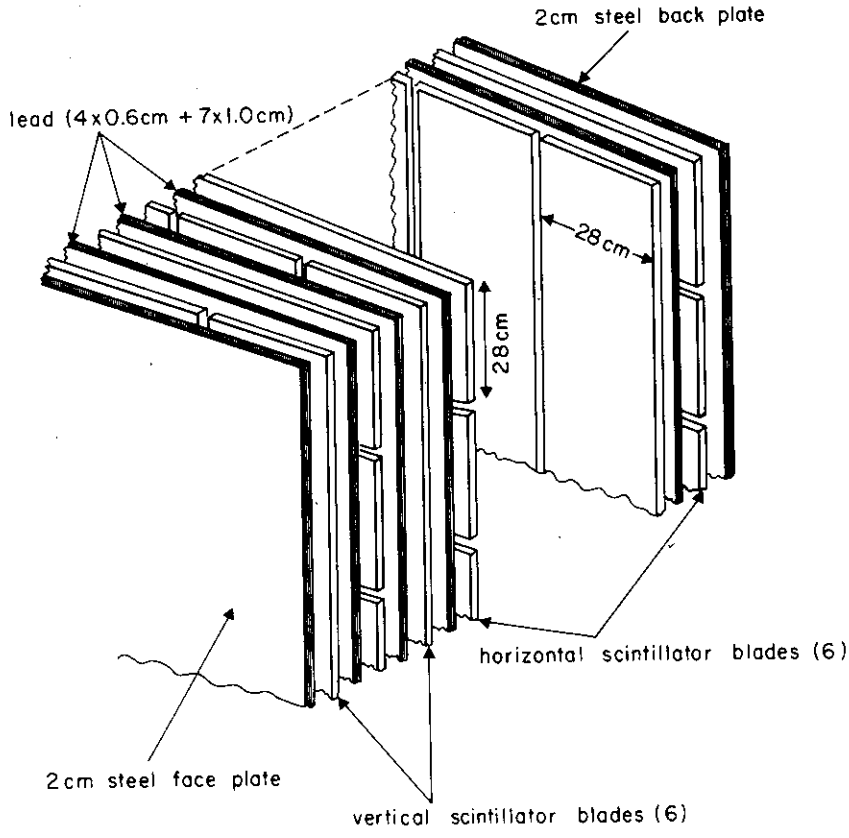
2cm steel back plate
lead (4x0.6cm + 7x1.0cm)
28cm
28cm
horizontal scintillator blades (6)
2cm steel face plate
vertical scintillator blades (6)

Fig. 9

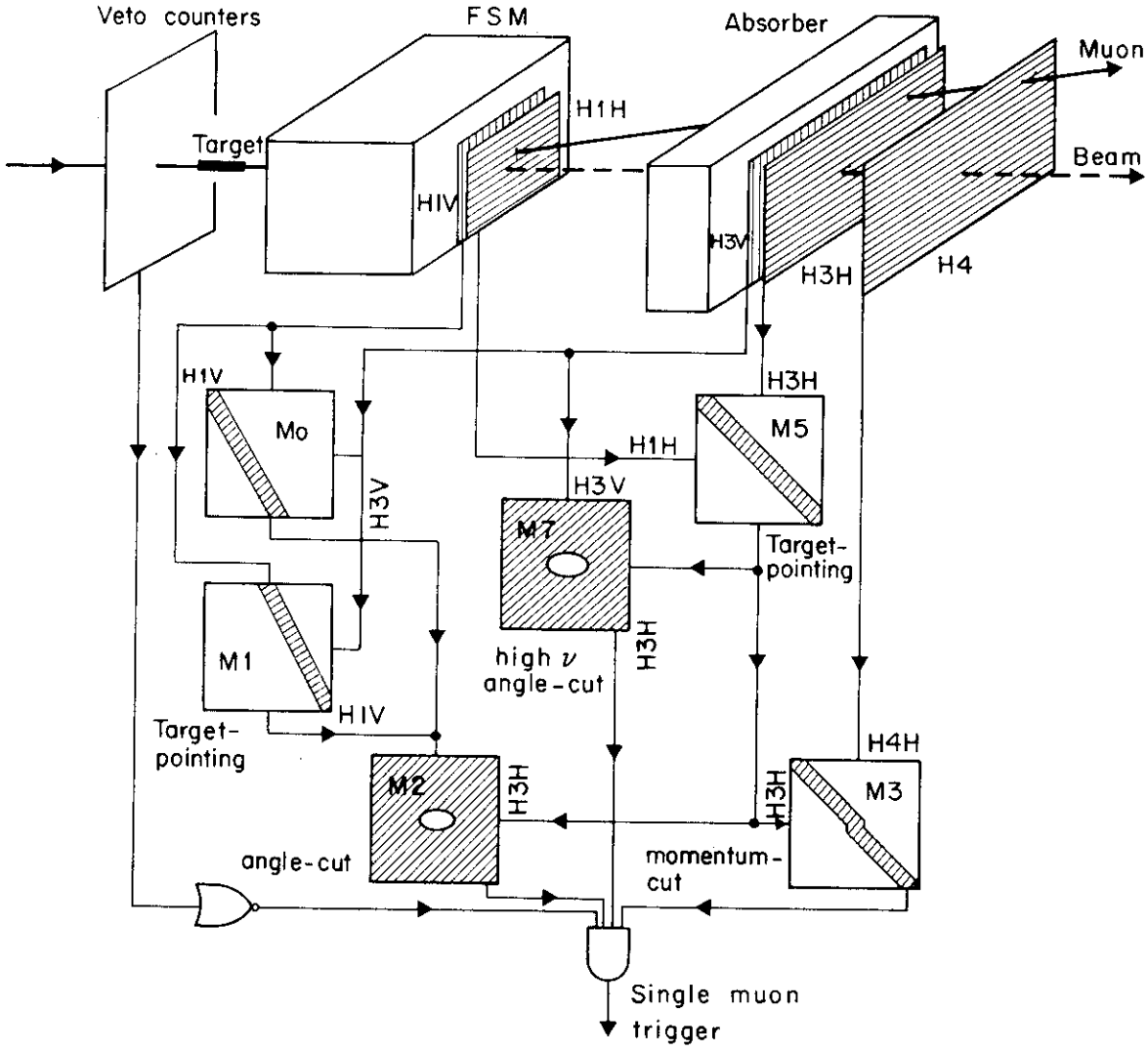
Veto counters
FSM
Absorber
Muon
Beam
Target
H1H
H1V
H3V
H3H
H4
Mo
M5
M7
M1
M2
M3
high ν
angle-cut
Target-
pointing
angle-cut
momentum-
cut
H4H
Single muon
trigger

Fig. 10

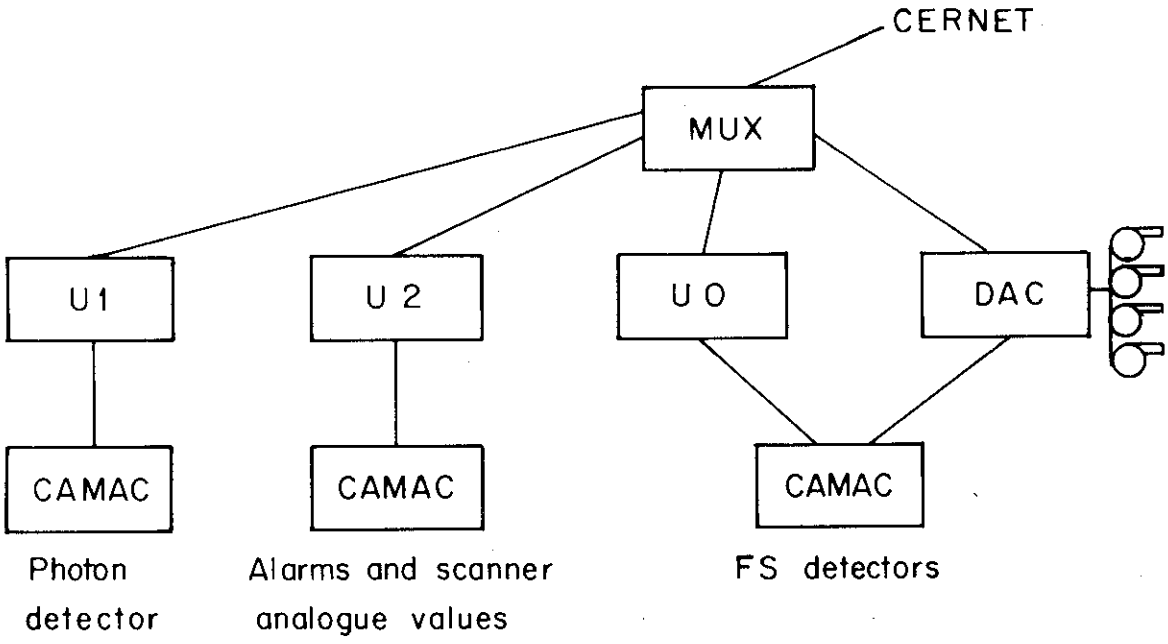
CERNET
MUX
U1
U 2
U O
DAC
CAMAC
CAMAC
CAMAC
Photon detector
Alarms and scanner analogue values
FS detectors

Fig. 11

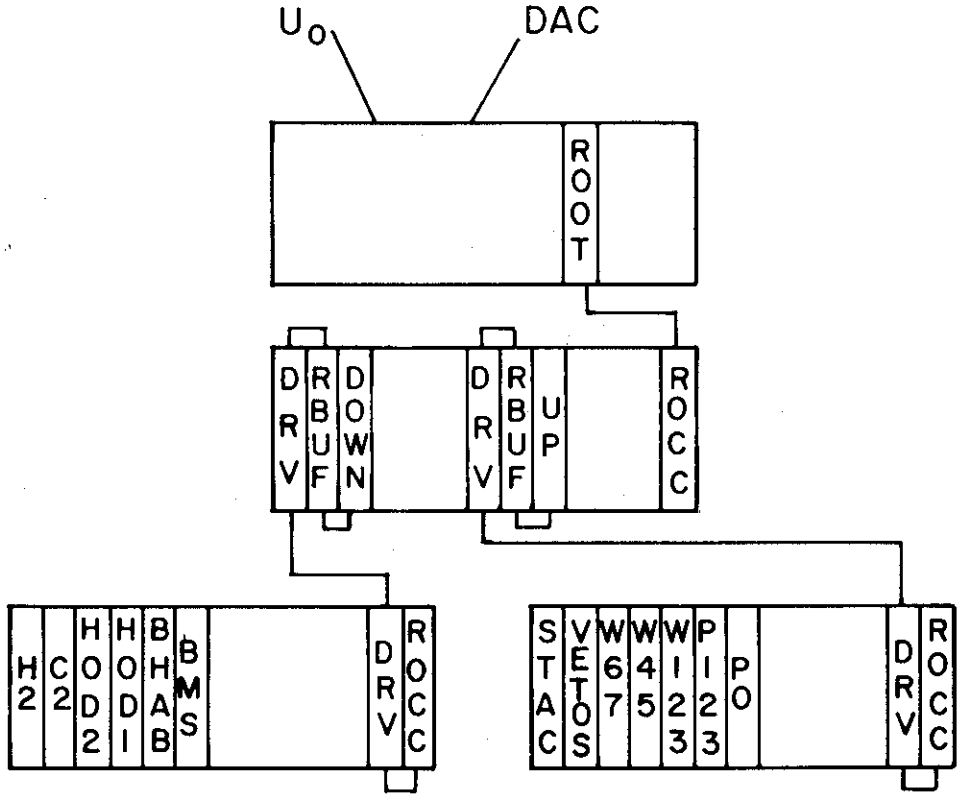
Uo
DAC
ROOT
DRV
RBUF
DOWN
DRV
RBUF
UP
ROCC
H2
C2
HOD2
HOD1
BHAB
BMS
DRV
ROCC
STAC
VETOS
W67
W45
WI23
PI23
PO
DRV
ROCC

Fig. 12

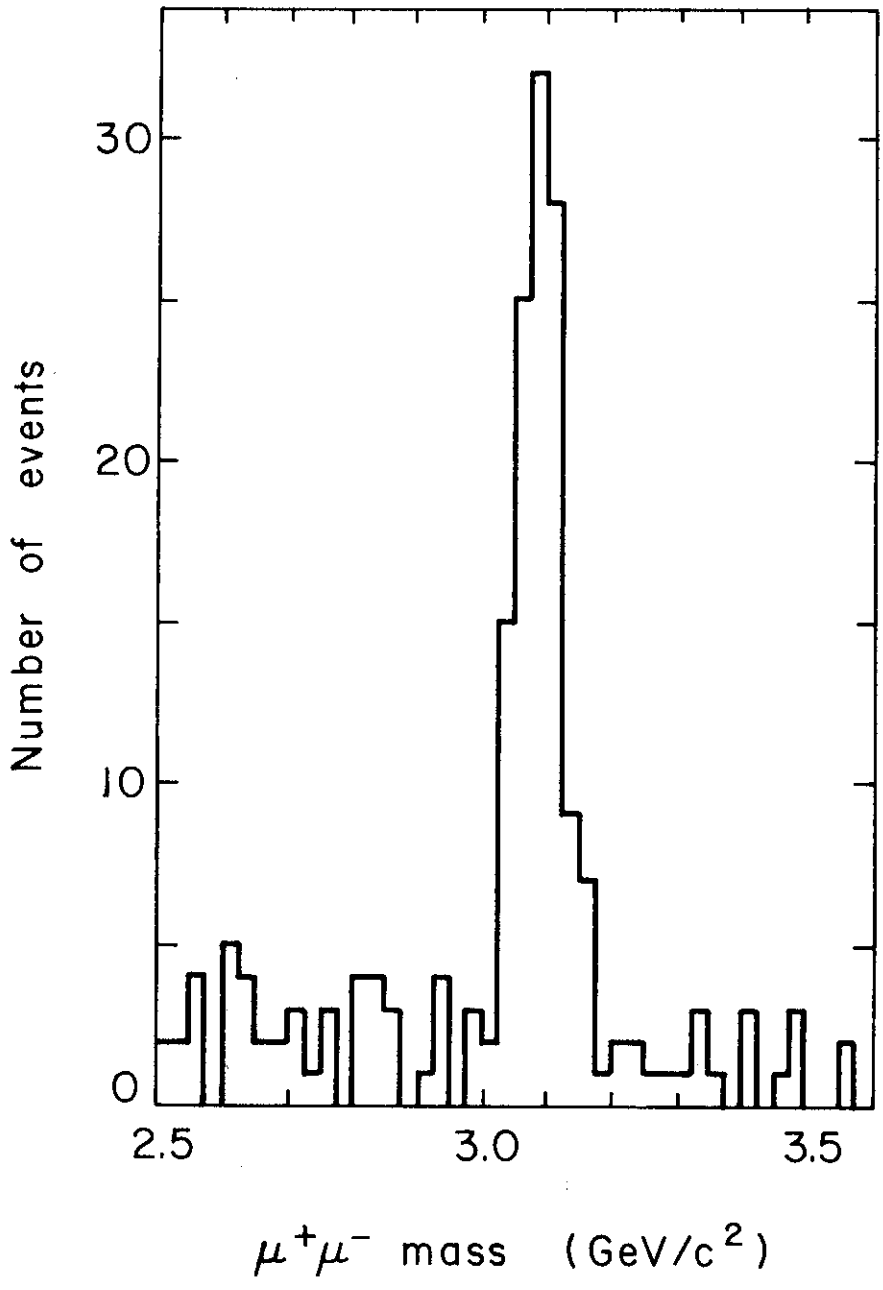

Fig. 13